Scheme 1. Chemical Structure and Synthesis of PCn

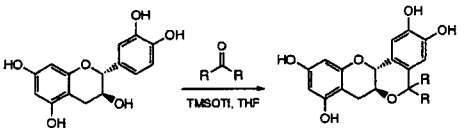

PC1 R = CH_3, *78.3% yield*
PC2 R = CH_2CH_3, *73.5% yield*
PC3 R = $(CH_2)_2CH_3$, *66.7% yield*
PC4 R = $(CH_2)_3CH_3$, *59.1% yield*
PC5 R = $(CH_2)_4CH_3$, *52.8% yield*
PC6 R = $(CH_2)_5CH_3$, *44.6% yield*

Scheme 2. Radical Scavenging Reaction of PCn against DPPH• and AAPH

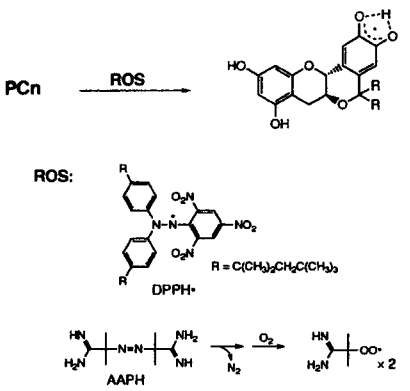

Table 1. Antioxidant Profile of Catechin and PCn Determined Using a DPPH and AAPH Scavenging Assay

compd	DPPH• k_{HT} (M^{-1} s^{-1})	AAPH IC_{50} (nM)
catechin	305	292
PC1	533	220
PC2	622	175
PC3	686	98
PC4	725	147
PC5	756	625
PC6	759	1700

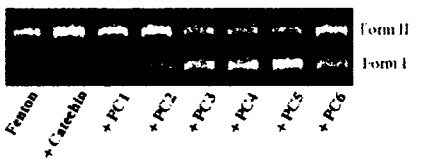

Figure 1. Effects of catechin and PCn on DNA breakage induced by the Fenton reaction (Fe^{3+}/H_2O_2). Assays were performed in 100 mM phosphate buffer, pH 7.0 containing 45 μM pBR322DNA, 10 mM H_2O_2, 100 μM $FeCl_3$, and 1 mM individual PCn for 1 h at 37 °C.

determined. Although **PC1** showed an excellent protecting effect against oxidative DNA scission compared with catechin,[3] the antioxidative activity of the series of **PCn** was evaluated under conditions in which the protecting effect of **PC1** appears to be weak. As shown in Figure 1, DNA cleaving activity induced by the Fenton reaction did not increase in the presence of **PCn**, and with an increase in the length of alkyl chains, the protecting effect of **PCn** on the oxidative DNA damage was greatly increased. The strong antioxidative activity might be attributed to a combination of radical scavenging activity and lipophilicity that tends to increase the binding between **PCn** and DNA. A small decrease in the protecting effect of **PC6** might be responsible for the diminishing radical scavenging ability under aqueous solution.

In addition to the antioxidative ability, (+)-catechin is known to be an inhibitor against α-glucosidase[7] that catalyzes the final

Table 2. Inhibitory Activities of Catechin and PCn against α-glucosidases

compd	*S. cerevisiae* IC_{50} (μM)	*B. stearothermophilus* IC_{50} (μM)
catechin	>500	>500
PC1	1.2	0.7
PC2	47.5	26.8
PC3	37.5	28.4
PC4	2.1	14.2
PC5	5.3	6.8
PC6	0.9	1.1

step in the digestive process of carbohydrates. Therefore, the inhibitory effects of **PCn** on α-glucosidase from *Saccharomyces cerevisiae* and *Bacillus stearothermophilus* were evaluated (Table 2). Surprisingly, in contrast to the relative weak inhibitory effect of (+)-catechin with IC_{50} > 500 μM, **PCn** exhibited strong inhibitory effects with IC_{50} = 0.7−47.5 μM against both enzymes, with **PC1** (IC_{50} = 1.2 μM for *S. cerevisiae* and 0.7 μM for *B. stearothermophilus*) and **PC6** (IC_{50} = 0.9 μM for *S. cerevisiae* and 1.1 μM for *B. stearothermophilus*) showing especially high inhibition concentrations. The strong inhibitory effect of **PCn** on α-glucosidase suggested that these planar catechin analogues may be used as a lead compounds for the development of antidiabetic therapeutics, similar to acarbose and voglibose which are known to reduce postprandial hyperglycemia primarily by interfering with the carbohydrate digesting enzymes and delaying glucose absorption.

In summary, a practical method for the preparation of planar catechin analogues with various alkyl side chain lengths is described as well as the remarkable properties of these compounds as potent antioxidants and α-glucosidase inhibitors. In vivo studies to fully exploit these potential benefits of PCn are currently under way, and the results will be published in due time.

Acknowledgment. This work was supported partly by a Grant from the Ministry of Health, Labor and Welfare, and by a Grant-in-Aid for Research of Health Sciences focusing on Drug Innovation (KH51058) from the Japan Health Sciences Foundation, partly by Grant-in-Aids for Scientific Research (B) (No. 17390033) and for Young Scientist (B) (No. 17790044) from the Ministry of Education, Culture, Sports, Science and Technology, Japan.

Note Added after ASAP Publication. After this paper was published ASAP on May 3, 2006, Table 2 was corrected to show the *S. cerevisiae* IC_{50} value of 1.2 μM for **PC1.**

Supporting Information Available: Experimental details. This material is available free of charge via the Internet at http://pubs.acs.org.

References

(1) (a) Raha, S.; Robinson, B. H. *Am. J. Med. Genet.* 2001, *106*, 62. (b) Kang, D.; Hamasaki, N. *Curr. Med. Chem.* **2005**, *12*, 429.
(2) Tsimilas, S.; Witztum, J. L. In *Oxidative stress and vascular diseases*; Keaney, J. F., Jr., Ed.; Kluwer: Boston, 2000; pp 49−74.
(3) Fukuhara, K.; Nakanishi, I.; Kansui, H.; Sugiyama, E.; Kimura, M.; Shimada, T.; Urano, S.; Yamaguchi, K.; Miyata, N. *J. Am. Chem. Soc.* **2002**, *124*, 5952.
(4) (a) Fukuhara, K.; Nakanishi, I.; Shimada, T.; Miyazaki, K.; Hakamata, W.; Urano, S.; Ikota, N.; Ozawa, T.; Okuda, H.; Miyata, N.; Fukuzumi, S. *Chem. Res. Toxicol.* **2003**, *16*, 81. (b) Nakanishi, I.; Ohkubo, K.; Miyazaki, K.; Hakamata, W.; Urano, S.; Ozawa, T.; Okuda, H.; Fukuzumi, S.; Ikota, N.; Fukuhara, K. *Chem. Res. Toxicol.* **2004**, *17*, 26.
(5) Joe, A. K.; Liu, H.; Suzui, M.; Vural, M. E.; Xiao, D.; Weinstein, I. B. *Clin. Cancer Res.* **2002**, *8*, 893.
(6) Krasowska, A.; Rosiak, D.; Szkapiak, K.; Oswiecimska, M.; Witek, S.; Lukaszewicz, M. *Cell. Mol. Biol. Lett.* **2001**, *6*, 71.
(7) Matsui, T.; Yoshimoto, C.; Osajima, K.; Oki, T.; Osajima, Y. *Biosci. Biotechnol. Biochem.* **1996**, *60*, 2019.

JA057763C

J. Appl. Glycosci., 53, 149–154 (2006)

Proceedings of the Symposium on Amylases and Related Enzymes, 2005

N-Linked Oligosaccharide Processing Enzymes as Molecular Targets for Drug Discovery

(Received December 1, 2005)

Wataru Hakamata,[1,*] Makoto Muroi,[2] Toshiyuki Nishio,[3] Tadatake Oku,[3] Akira Takatsuki,[4] Hiroyuki Osada,[2] Kiyoshi Fukuhara,[1] Haruhiro Okuda[1] and Masaaki Kurihara[1]

[1]*Division of Organic Chemistry, National Institute of Health Sciences (NIHS) (1–18–1, Kamiyoga, Setagaya-ku, Tokyo 158–8501, Japan)*
[2]*Antibiotics Laboratory, The Institute of Physical and Chemical Research (RIKEN) (2–1, Hirosawa, Wako, Saitama 351–0198, Japan)*
[3]*Department of Biological Chemistry, College of Bioresource Sciences, Nihon University (1866, Kameino, Fujisawa, Kanagawa 252–8510, Japan)*
[4]*Department of Materials Chemistry, Faculty of Engineering, Hosei University (3–7–2, Kajino-cho, Koganei, Tokyo 184–8584, Japan)*

Abstract: *N*-Linked oligosaccharide processing enzymes are key enzymes in the biosynthesis of *N*-linked oligosaccharides. These enzymes are a molecular target for inhibition by anti-viral agents that interfere with the formation of essential glycoproteins required in viral assembly, secretion and infectivity. We think that the molecular recognition of three kinds of glucosidases (family 13 and family 31 α-glucosidases and endoplasmic reticulum glucosidases) are different. Therefore, glycon and aglycon specificity profiling of glucosidases was an important approach for the research of glucosidase inhibitors. We carried out the profiling of glucosidases using small molecules as a probe. Moreover, we designed and synthesized three types of glucosidase inhibitors. These compounds were evaluated with regard to their ability to inhibit glucosidases *in vitro*, and were also tested in a cell culture system. We found some compounds having glucosidase inhibitory activity and anti-viral activity.

Key words: α-glucosidase, ER glucosidase, inhibitor, anti-viral activity

α-Glucosidases (EC 3.2.1.20) are also exo-acting carbohydrases, catalyzing the release of α-D-glucopyranose from the non-reducing ends of various substrates,[1,2] and on the basis of amino acid sequence similarities, α-glucosidases are classified into two families, family 13 and family 31.[3,4] Endoplasmic reticulum (ER) glucosidases, glucosidase I (EC 3.2.1.106) and glucosidase II (EC 3.2.1.84), are key enzymes in the biosynthesis of asparagine-linked oligosaccharides that catalyze the first processing event after the transfer of $Glc_3Man_9GlcNAc_2$ to proteins. These enzymes are a target for inhibition by anti-viral agents that interfere with the formation of essential glycoproteins required in viral assembly, secretion and infectivity.[5] Many papers reported that inhibitors of α-glucosidases are potential therapeutics for the treatment of such diseases as viral diseases, cancer and diabetes.[5,6] However, many screenings of α-glucosidase inhibitors did not use enzymes from target tissues or organs. We think that the molecular recognitions of three kinds of glucosidases (family 13, family 31 α-glucosidases and ER glucosidases) are different. Therefore, the glycon and aglycon specificity profiling of glucosidases has been an important approach for the research of glucosidase inhibitors.

In this research, we first describe the glycon and aglycon specificity profiling of glucosidases using small molecules as probes. Next, compounds designed and synthesized as glucosidase inhibitor candidates were evaluated with regard to their ability to inhibit three kinds of glucosidases. Finally, the glucosidase inhibitor candidates were tested for their anti-viral activities in a cell culture system.

*Corresponding author (Tel. +81–3–3700–1141, Fax. +81–3–3707–6950, E-mail: hakamata@nihs.go.jp).

Glycon specificity profiling of glucosidases using chemically modified substrates.

Chemically modified substrates are effective methods in the study of substrate specificity profiling. We have applied this approach to family 13 and family 31 α-glucosidases,[7–10] ER glucosidases,[11,12] α-galactosidases[8,13] and α-mannosidases[8,14] using partially substituted monosaccharides. We used all of the monodeoxy analogs of *p*-nitrophenyl α-D-glucopyranoside (PNP α-Glc) **1–4** (Fig. 1) as chemically modified substrates for glycon specificity profiling. We investigated the hydrolytic activities of family 13 and family 31 α-glucosidases and ER glucosidase II of PNP α-Glc and its deoxy derivatives **1–4**, and checked the inhibitory activities of ER glucosidase I of PNP α-Glc and probes **1–4**, so that PNP α-Glc was not a substrate for ER glucosidase I. These results are shown in Table 1.[11,12] Clearly, of the four deoxy derivatives of PNP α-Glc **1–4**, family 31 α-glucosidases and ER glucosidase II hydrolyzed the 2-deoxy glucopyranoside (**1**); its activity with **1** appeared to be substantially higher than that with PNP α-Glc. Kinetic studies of the hydrolysis of PNP α-Glc, **1** and **2** were also carried out (Table 2).[9,11] The V_{max}/K_m or k_{cat}/K_m values of family 31 α-glucosidases

and ER glucosidase II for **1** was about twice as great as PNP α-Glc, which indicated that probe **1** was a good substrate for the enzymes. These reaction velocities to probe **1** increased to 3–28 fold that of PNP α-Glc. PNP Glc and probes **1**–**4** inhibited ER glucosidase I by 56.2, 71.7, 18.5, 22.2 and 32.3% at 5 mM, respectively. These results also indicated that ER glucosidase II might have properties similar to those found in family 31 α-glucosidases.

Aglycon specificity profiling and inhibition of glucosidases using heptitol derivatives.

For aglycon specificity profiling, we designed and synthesized eight probes, **5**–**12**, including 1-amino-2, 6-anhydro-1-deoxy-D-*glycero*-D-*ido*-heptitol, which might mimic to a great extent the topography of α-D-glucopyranoside and modified aglycon of α-glucopyranoside (Fig. 2).[11] These probes do not have the specific functional groups for glycosidase inhibition, electrostatic interactions (*e.g.* 1-deoxynojirimycine), transition state mimetic structure (*e.g.* D-gluconolactone), or covalent bond formation with the enzyme catalytic site (*e.g.* conduritol B epoxide). The structures of α-glucosidase inhibitors are summarized in Fig. 3. We investigated the inhibitory activities of family 13 and family 31 α-glucosidases, ER glucosidases, and other glycosidases (β-glucosidase, α- and β-mannosidase, α- and β-galactosidase) against probes

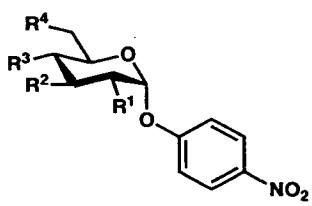

1: R^1=H, R^2=R^3=R^4=OH
2: R^1=R^3=R^4=OH, R^2=H
3: R^1=R^2=R^4=OH, R^3=H
4: R^1=R^2=R^3=OH, R^4=H

Fig. 1. Chemical structure of glycon profiling probes **1**–**4**.

5–**12**, and their aglycon specificity profiling was discussed. The values of the % inhibition and IC_{50} are summarized in Table 3.[12] Probe **8** indicated specific inhibitions of *Saccharomyces* (*S.*) *cerevisiae* (IC_{50}=55.5 μM) and *Bacillus* (*B.*) *stearothermophilus* (IC_{50}=415 μM) α-glucosidases. Probe **11** inhibited α-glucosidase from *S. cerevisiae* (IC_{50}=449 μM). Honey bee isozyme I (HBG I) was inhibited by probe **5** (IC_{50}=851 μM). Family 13 α-glucosidases and ER glucosidases were inhibited by the specific probes. On the other hand, family 31 α-glucosidases were broadly inhibited by probes **5**–**12**. All probes did not inhibit β-glucosidase, α- or β-mannosidases, or α- or β-galactosidases at a 5-fold concentration. These facts indicated that aglycon specificities of α-glucosidases differed greatly among family 13 α-glucosidases, family 31 α-glucosidases and ER glucosidases. Moreover, each aglycon specificity of family 13 α-glucosidases is different in spite of the highly conserved amino acid sequences in the catalytic site.[15] In the kinetic studies on the inhibitions of **8** and **11** and the hydrolysis of PNP α-Glc by *S. cerevisiae* and *B. stearothermophilus* α-glucosidases, the values of K_i and K_m (mM) were calculated from Dixon plots and Michaelis-Menten plots, respectively, and these values and inhibition types are summarized in Table 4.[12] Probes **8** and **11** were competitive type inhibitors of the *S. cerevisiae* enzyme (K_i=0.13 mM and 0.50 mM). Probe **8** was a mixed type inhibitor of *B. stearothermophilus* enzyme (K_i=0.58 mM). The affinities of **8** against both enzymes were higher than PNP α-Glc as a substrate. These results indicated that probe **8** formed a specific hydrogen bond between the primary hydroxyl group of aglycon moiety and *S. cerevisiae* enzyme, and that probe **11**, with a terminal phenyl group, formed a hydrophobic interaction with the *S. cerevisiae* enzyme.

Inhibition of α-glucosidase by reactive oxygen species.

The reactive oxygen species (ROS) generated com-

Table 1. Hydrolytic activities and inhibitory activities of probes **1**–**4** against glucosidases.[11,12]

Enzyme source	Relative rate of hydrolysis (%) / % Inhibition				
	PNP α-Glc	PNP 2D α-Glc (1)	PNP 3D α-Glc (2)	PNP 4D α-Glc (3)	PNP 6D α-Glc (4)
ER Processing glucosidase					
Rat microsome					
Glucosidase I	– / 56.2	– / 71.7	– / 18.5	– / 22.2	– / 32.3
Glucosidase II	100 / HD	189 / HD	– / –	– / –	– / –
	Relative rate of hydrolysis (%)				
α-Glucosidase family 13					
S. cerevisiae	100	–	–	–	–
B. stearothermophilus	100	–	–	–	–
Honey bee I	100	–	–	–	–
Honey bee II	100	–	–	–	–
Honey bee III	100	–	–	–	–
α-Glucosidase family 31					
Rice	100	175	–	–	–
Sugar beet	100	244	–	–	–
Flint corn	100	231	3.7	–	–
A. niger	100	259	11.9	–	–

Relative rate of hydrolysis was expressed by comparison with the amount of *p*-nitrophenol that was released from PNP α-Glc, which was taken as 100%. Assay of glucosidase I inhibitory activities used [^{3}H] glucose-labeled VSV glycoprotein as a substrate. –, Hydrolytic or inhibitory activity was not detected, HD, Hydrolyzing activity was observed.

Table 2. Kinetic study of hydrolysis of family 31 α-glucosidases and ER glucosidase II.[9,11]

Enzyme / Substrate	K_m (mM)	V_{max} (μmol/min/U)	V_{max}/K_m
ER glucosidase II			
PNP α-Glc	0.92	1.12	1.23
PNP 2D α-Glc (**1**)	0.76	3.44	4.53
Enzyme / Substrate	K_m (mM)	k_{cat} (s^{-1})	k_{cat} / K_m
Rice α-glucosidase			
PNP α-Glc	2.62	43.8	16.7
PNP 2D α-Glc (**1**)	6.66	237	35.6
Sugar beet α-glucosidase			
PNP α-Glc	1.04	0.071	0.068
PNP 2D α-Glc (**1**)	5.70	0.64	0.11
Flint corn α-glucosidase			
PNP α-Glc	0.88	2.00	2.27
PNP 2D α-Glc (**1**)	7.38	17.0	2.30
PNP 3D α-Glc (**2**)	9.98	0.44	0.044
A. niger α-glucosidase			
PNP α-Glc	0.59	3.44	5.83
PNP 2D α-Glc (**1**)	6.09	96.9	15.9
PNP 3D α-Glc (**2**)	10.2	4.23	0.41

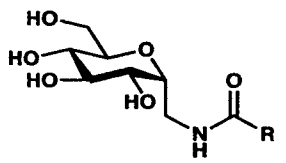

5: R=CH_2OH **9**: R=$(CH_2)_5OH$
6: R=$(CH_2)_2OH$ **10**: R=Me
7: R=$(CH_2)_3OH$ **11**: R=Ph
8: R=$(CH_2)_4OH$ **12**: R=$C(CH_3)_3$

Fig. 2. Chemical structure of aglycon profiling probes **5**–**12**.

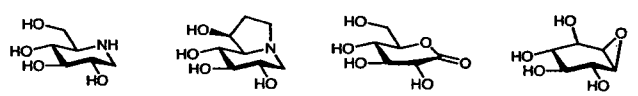

1-deoxynojirimycine castanospermine D-gluconolactone conduritol B epoxide

Fig. 3. Chemical structure of typical α-glucosidase inhibitor.

pounds, **13**–**24**, shown in Fig. 4, were assessed as inhibitors of glycoside hydrolase family 13 α-glucosidases and family 31 α-glucosidases,[16] and the results are listed in Table 5 (Preparation for publication). Compounds **18** and **24**, with a terminal α-naphthyl group, indicated inhibitions of α-glucosidases from *S. cerevisiae* (IC_{50}=51.7 μM and IC_{50}=74.1 μM) and *B. stearothermophilus* (IC_{50}=60.1 μM and IC_{50}=89.1 μM). We reasoned that the enzymatic liberation of the aglycon from compounds **18** and **24** might be followed by the ejection of a sulfinate anion with the concomitant formation of *p*-benzoquinone and *p*-benzoquinone imine, which would then generate ROS in the enzyme active site, leading to enzyme deactivation.[16,17] Therefore, the effects of compounds **18** and **24** on ROS-mediated DNA breakage were investigated. DNA strand scission in the super coiled pBR322DNA was induced by ROS in the presence of *p*-benzoquinone or *p*-benzoquinone imine, metal ion, and NADH.[17] Compound **24** induced DNA strand breakage condition in the above conditions (data not shown). We suggest that ROS-generated enzyme inhibition might be a new approach for the development of an enzyme inhibitor.

Inhibition of α-glucosidase by catechin derivatives. The catechin derivatives **25**–**33** shown in Fig. 5 were assessed as inhibitors of family 13 and family 31 α-glucosidases, and the results are listed in Table 6.[18] A comparison of the results against family 13 and family 31 α-glucosidases shows that family 13 α-glucosidases were remarkably inhibited by catechin derivatives compared with family 31 α-glucosidases. The potent inhibition of family 13 α-glucosidases, *S. cerevisiae* and *B. stearothermophilus*, shown by catechin derivative **25** (IC_{50}=1.2 μM and IC_{50}=0.7 μM) and **30** (IC_{50}=0.9 μM and IC_{50}=1.1 μM), are in contrast to the weak activity shown by cate-

Table 3. Inhibitory activities of probes **5**–**12** against glycosidases.[12]

Enzyme source	% Inhibition (IC_{50})							
	5	**6**	**7**	**8**	**9**	**10**	**11**	**12**
Family 13 α-glucosidase								
S. cerevisiae	<1.0	21.1	<1.0	100 (55.5 μM)	<1.0	<1.0	67.4 (449 μM)	6.1
B. stearothermophilus	<1.0	<1.0	<1.0	100 (415 μM)	<1.0	<1.0	<1.0	<1.0
Honey bee I	52.3 (851 μM)	<1.0	<1.0	37.5	<1.0	10.4	4.6	<1.0
Honey bee II	4.4	2.7	3.6	21.4	4.4	<1.0	12.3	<1.0
Honey bee III	<1.0	3.2	<1.0	<1.0	<1.0	<1.0	<1.0	<1.0
Family 31 α-glucosidase								
Rice	10.7	8.5	7.6	18.3	26.0	21.8	16.0	3.8
Sugar beet	6.9	1.7	3.6	3.1	11.9	8.8	9.8	3.2
Flint corn	29.1	14.1	18.5	37.0	44.6	31.0	49.2	5.6
A. niger	6.6	2.6	<1.0	6.8	<1.0	23.3	14.0	1.2
ER processing glucosidase								
Glucosidase I	<1.0	<1.0	<1.0	<1.0	<1.0	<1.0	18.2	<1.0
Glucosidase II	<1.0	<1.0	<1.0	<1.0	<1.0	<1.0	5.9	<1.0
β-Glucosidase	<1.0	<1.0	<1.0	<1.0	<1.0	<1.0	<1.0	<1.0
α-Mannosidase	<1.0	<1.0	<1.0	<1.0	<1.0	<1.0	<1.0	<1.0
β-Mannosidase	<1.0	<1.0	<1.0	<1.0	<1.0	<1.0	<1.0	<1.0
α-Galactosidase	<1.0	<1.0	<1.0	<1.0	<1.0	<1.0	<1.0	<1.0
β-Galactosidase	<1.0	<1.0	<1.0	<1.0	<1.0	<1.0	<1.0	<1.0

Probe concentrations (family 13 and 31 α-glucosidases: 1 μmol/mL, ER processing α-glucosidases: 2 μmol/mL, β-glucosidase, mannosidases and galactosidases: 5 μmol/mL). Substrate (family 13 and 31 α-glucosidases, ER glucosidase II: PNP α-Glc, ER glucosidases I: [^{3}H] glucose-labeled vesicular stomatitis virus glycoprotein, β-glucosidase: PNP β-Glc, α-mannosidase: PNP α-Man, β-mannosidase: PNP β-Man, α-galactosidase: PNP α-Gal, β-galactosidase: PNP β-Gal).

Table 4. Kinetic studies of the inhibition of family 13 α-glucosidases.[12]

Probe	*S. cerevisiae*		*B. stearothermophilus*	
	*K*i (mM)	Inhibition type	*K*i (mM)	Inhibition type
8	0.13	Competitive	0.58	Mixed
11	0.50	Competitive	–	–
PNP α-Glc	0.35*	–	1.16*	–

*K_m value.

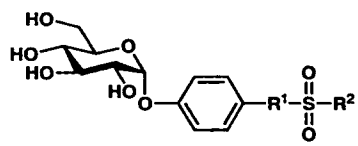

13: R^1=O, R^2=NO_2
14: R^1=O, R^2=Cl
15: R^1=O, R^2=CF_3
16: R^1=O, R^2=CH_3
17: R^1=O, R^2=$C(CH_3)_3$
18: R^1=O, R^2=α-naphthyl
19: R^1=NH, R^2=NO_2
20: R^1=NH, R^2=Cl
21: R^1=NH, R^2=CF_3
22: R^1=NH, R^2=CH_3
23: R^1=NH, R^2=$C(CH_3)_3$
24: R^1=NH, R^2=α-naphthyl

Fig. 4. Chemical structure of ROS-generated compounds **13**–**24**.

Table 5. Inhibitory activity of ROS-generated compounds **13**–**24** against α-glucosidases.

Compound	IC_{50} (μM)		
	Glycoside hydrolase family 13		Glycoside hydrolase family 31
	S. cerevisiae	*B. stearothermophilus*	Rice
13	499	>500	>500
14	437	>500	>500
15	407	>500	>500
16	499	>500	>500
17	391	>500	>500
18	51.7	60.1	>500
19	239	218	>500
20	200	254	>500
21	146	244	>500
22	231	325	>500
23	136	237	>500
24	74.1	89.1	>500

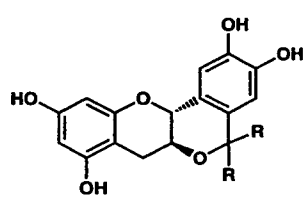

25: R=CH_3
26: R=CH_2CH_3
27: R=$(CH_2)_2CH_3$
28: R=$(CH_2)_3CH_3$
29: R=$(CH_2)_4CH_3$
30: R=$(CH_2)_5CH_3$
31: R=$(CH_2)_6CH_3$
32: R=$(CH_2)_7CH_3$
33: R=$(CH_2)_8CH_3$

Fig. 5. Chemical structure of catechin derivatives **25**–**33**.

chin derivative **26**, which has one methylene group long alkyl side chain compared with **25** (IC_{50}=47.5 μM and IC_{50}=26.8 μM) and catechin derivative **33** which has three methylene groups long alkyl side chain compared with **30** (IC_{50}=64.0 μM and IC_{50}=28.1 μM). From these results, it is thought that the inhibition mechanism of catechin derivative **25** and the inhibition mechanism of catechin derivative **30** are different. The IC_{50} values of typical α-glucosidase inhibitor 1-deoxynojirimycine (see Fig. 3) and catechin derivative **30** against *S. cerevisiae* α-glucosidase

Table 6. Inhibitory activity of catechin derivatives **25**–**33** against α-glucosidases.[18]

Compound	IC_{50} (μM)			
	Glycoside hydrolase family 13		Glycoside hydrolase family 31	
	S. cerevisiae	*B. stearothermophilus*	Rice	*A. niger*
Catechin	>500	>500	>500	>500
25	1.2	0.7	>500	>500
26	47.5	26.8	>500	>500
27	37.5	28.4	>500	>500
28	2.1	14.2	>500	>500
29	5.3	6.8	248	>500
30	0.9	1.1	>500	>500
31	4.9	21.1	>500	>500
32	33.2	13.8	>500	>500
33	64.0	28.1	>500	>500

were 3.3[19] and 0.9 μM, respectively. This result indicated that catechin derivative **30** is about 3.6 times more potent than 1-deoxynojirimycine when their IC_{50} values are compared.

Anti-viral activity of α-glucosidase inhibitors.

Compounds **1**–**33** were assayed with regard to their ability to inhibit glycoprotein processing at the cellular level. Vesicular stomatitis virus glycoprotein (VSV G) was prepared from VSV-infected and probe-treated baby hamster kidney (BHK) cells.[11] Analyses of the *N*-glycan structure of obtained VSV G using endo H, which is known to have hydrolytic activity against high-mannose type *N*-glycan, failed to confirm that compounds **1**–**24** except for catechin derivatives (**25**–**33**) inhibited processing glycosidases. The catechin derivatives had the possibility of inhibition of processing glycosidases (data not shown). Then, we assayed the anti-virus activities by effects of the catechin derivatives of processing glycosidases on virus glycoprotein synthesis and syncytium formation after newcastle disease virus (NDV) infection, and effects on synthesis and cell surface expression of NDV glycoprotein, hemagglutinin-neuraminidase (HANA) glycoprotein in whole cell lysates were quantified. Moreover, viral infectivity was determined by a plaque assay in BHK cells.[20] In the above assays, catechin derivative **30** showed potent inhibition of the viral infectivity (Table 7, Preparation for publication).

Conclusion and perspectives.

The discovery of glucosidase inhibitors may help us to understand the roles of the oligosaccharides of glycoproteins and glycolipids in cellular functions, and pharmaceutical applications. From this study, it is better to use enzymes of target tissues or organs for the screening of agents for viral diseases, cancer and diabetes. Moreover, in applying glucosidases as inhibitors of glycoprotein processing, inhibitory action of many inhibitors at the cellular levels is not so remarkable, as expected based on their action at the enzyme level. This was speculated to be caused by the difficulty for inhibitors to be able to access the site of action. We think that high throughput

Table 7. Anti-viral activity of catechin derivatives at the cellular level.

Compound	Conc. (μM)	% HAU	SF	% PFU	CPU
Catechin	500	100	+	95	+
	250	100	+	100	+
	125	100	+	NT	+
	63	100	+	NT	+
25	500	0	−	0	+
	250	6	−	14	+
	125	100	+	100	+
	63	100	+	100	+
26	500	0	−	0	−
	250	0	−	0	+
	125	100	+	24	+
	63	100	+	85	+
27	500	0	−	0	−
	250	0	−	0	−
	125	0	−	0	−
	63	100	+	90	+
28	500	0	−	0	−
	250	0	−	0	−
	125	0	−	0	−
	63	100	+	90	+
29	500	0	−	0	−
	250	0	−	0	−
	125	0	−	0	−
	63	100	+	50	−
	31	100	+	100	+
	16	100	+	100	+
30	500	0	−	0	−
	250	0	−	0	−
	125	0	−	0	−
	63	9	+/−	25	−
	31	100	+	95	+
	16	100	+	100	+
33	500	0	−	0	−
	250	0	−	0	−
	125	25	−	50	−
	63	100	+	100	+

screening assays using specific probes and enzymes of target tissues or organs and highly effective design and synthesis of inhibitors *in silico* are necessary for the development of new and potent glucosidase inhibitors.

The authors express sincere thanks to Dr. Seiya Chiba and Dr. Atsuo Kimura for their advice and for some of the α-glucosidases. We thank Ezaki Glico Co., Ltd. for the gift of α-arbutin. This work was performed at the Special Postdoctoral Researchers Program (RIKEN). This research was partially supported by a Ministry of Education, Science, Sports and Culture, Grant-in-Aid for Young Scientists (B), 17790097, 2005.

REFERENCES

1) S. Chiba: *Handbook of Amylases and Related Enzymes*, Amylase Research Society of Japan, eds., Pergamon, Oxford, pp. 104–116 (1988).
2) T.P. Frandesn and B. Svensson: Plant α-glucosidases of the glycoside hydrolase family 31. Molecular properties, substrate specificity, reaction mechanism, and comparison with family members of different origin. *Plant Molecul. Biol.*, **37**, 1–13 (1998).
3) G.J. Davies and B. Henrissat: Structural enzymology of carbohydrate-active enzymes: implications for the post-genomicera. *Biochem. Soc. Trans.*, **30**, 291–297 (2001).
4) Y. Bourne and B. Henrissat: Glycoside hydrolases and glycosyltransferases: families and functional modules. *Curr. Opin. Struct. Biol.*, **11**, 593–600 (2001).
5) A. Mehta, N. Zitzmann, P.M. Rudd, T.M. Block, R.A. Dwek: α-Glucosidase inhibitors as potential broad based anti-viral agents. *FEBS Lett.*, **430**, 17–22 (1998).
6) R.A. Dwek, T.D. Butters, F.M. Platt and N. Zitzmann: Targeting glycosylation as a therapeutic approach. *Nat. Rev. Drug Discovery*, **1**, 65–75 (2002).
7) W. Hakamata, T. Nishio and T. Oku: Synthesis of *p*-nitrophenyl 3- and 6-deoxy-α-D-glucopyranosides and their specificity to rice α-glucosidase. *J. Appl. Glycosci.*, **46**, 459–463 (1999).
8) W. Hakamata, T. Nishio, R. Sato, T. Mochizuki, K. Tsuchiya, M. Yasuda and T. Oku: Synthesis of monomethyl derivatives of *p*-nitrophenyl α-D-gluco, galacto, and mannopyranosides and their hydrolytic properties against α-glycosidase. *J. Carbohydr. Chem.*, **19**, 359–377 (2000).
9) T. Nishio, W. Hakamata, A. Kimura, S. Chiba, A. Takatsuki, R. Kawachi and T. Oku: Glycon specificity profiling of α-glucosidases using monodeoxy and mono-*O*-methyl derivatives of *p*-nitrophenyl α-D-glucopyranoside. *Carbohydr. Res.*, **337**, 629–634 (2002).
10) T. Nishio, W. Hakamata, M. Ogawa, K. Nakajima, Y. Matsuishi, R. Kawachi and T. Oku: Investigations of useful α-glycosidase for the enzymatic synthesis of rare sugar oligosaccharides. *J. Appl. Glycosci.*, **52**, 153–160 (2005).
11) W. Hakamata, M. Muroi, T. Nishio, T. Oku and A. Takatsuki: Recognition properties of processing α-glucosidase I and α-glucosidase II. *J. Carbohydr. Chem.*, **23**, 27–39 (2004).
12) W. Hakamata, M. Muroi, K. Kadokura, T. Nishio, T. Oku, A. Kimura, S. Chiba and A. Takatsuki: Aglycon specificity profiling of α-glucosidases using synthetic probes. *Bioorg. Med. Chem. Lett.*, **15**, 1489–1492 (2005).
13) W. Hakamata, T. Nishio and T. Oku: Hydrolytic activity of α-galactosidase against deoxy derivatives of *p*-nitrophenyl α-D-galactopyranoside. *Carbohydr. Res.*, **324**, 107–115 (2000).
14) T. Nishio, Y. Miyake, H. Tsujii, W. Hakamata, K. Kadokura and T. Oku: Hydrolytic activity of α-mannosidase against deoxy derivatives of *p*-nitrophenyl α-D-mannopyranoside. *Biosci. Biotechnol. Biochem.*, **60**, 2038–2042 (1996).
15) A. Kimura: Molecular anatomy of α-glucosidase, *Trends Glycosci. Glycotechnol.*, **12**, 373–380 (2000).
16) J.C. Briggs, A.H. Haines and R.J.K. Taylor: 4-(Sulfonylamino) phenyl α-D-glucopyranosides as competitive inhibitors of yeast α-glucosidase. *J. Chem. Soc., Chem. Commun.*, **18**, 1410–1411 (1993).
17) K. Fukuhara, I. Nakanishi, H. Kansui, E. Sugiyama, M. Kimura, T. Shimada, S. Urano, K. Yamaguchi and N. Miyata: Enhanced radical-scavenging activity of a planar catechin analogue. *J. Am. Chem. Soc.*, **124**, 5952–5953 (2002).
18) W. Hakamata, I. Nakanishi, Y. Masuda, T. Shimizu, H. Higuchi, Y. Nakamura, T. Oku, S. Saito, S. Urano, T. Ozawa, N. Ikota, N. Miyata, H. Okuda and K. Fukuhara: Planar catechin analogues with alkyl side chain, a potent antioxidant and α-glucosidase inhibitor. *J. Am. Chem. Soc.* (2006). (in press)
19) A.B. Hughes and A.J. Rudge: Deoxynojirimycin: synthesis and biological activity. *Nat. Prod. Rep.*, **11**, 135–162 (1994).
20) E. Tsujii, M. Muroi, N. Shiragami and A. Takatsuki: Nectrisine is a potent inhibitor of α-glucosidases, demonstrating activities similarly at enzyme and cellular levels. *Biochem. Biophys. Res. Commun.*, **220**, 459–466 (1996).

N-結合型糖鎖プロセッシング酵素を分子標的とした創薬

袴田 航[1], 室井 誠[2], 西尾俊幸[3], 奥 忠武[3], 高月 昭[4], 長田裕之[2], 福原 潔[1], 奥田晴宏[1], 栗原正明[1]

[1] 国立医薬品食品衛生研究所有機化学部
(158-8501 東京都世田谷区上用賀 1-18-1)
[2] 理化学研究所長田抗生物質研究室
(351-0198 和光市広沢 2-1)
[3] 日本大学生物資源科学部農芸化学科
(252-8510 藤沢市亀井野 1866)
[4] 法政大学工学部生命機能科学科
(184-8584 小金井市梶野町 3-7-2)

現在，新H5N1型インフルエンザやSARSなど続々と出現する新興ウイルス感染症や鳥インフルエンザのヒトへの伝播等，新興ウイルス感染症は人類の脅威となっている．しかし，ウイルス感染症に対する有効な薬剤の開発は，細菌感染症の抗生物質に比べ遅れている．そこで，ウイルス共通の感染機序に基づいた薬剤の開発が重要と考え，外被を有する多くのウイルスの感染・増殖には複合型の*N*-結合型糖鎖が関与している知見を基にして，小胞体*N*-結合型糖鎖プロセシング酵素を標的酵素とした分子標的薬の開発を目指して研究を行っている．分子標的薬の開発には，標的酵素である糖鎖プロセシング酵素の基質特異性の解明が必要であると考えた．そこで，合成プローブを用いて*N*-結合型糖鎖プロセシングの第1段階を担うプロセシンググルコシダーゼI (EC 3.2.1.106)と第2段階を担うプロセシンググルコシダーゼII (EC 3.2.1.84)のグリコンおよびアグリコン特異性を調べ，α-グルコシダーゼ (EC 3.2.1.20, GH13 and GH31) のそれと比較した．その結果，グルコシダーゼIのグリコン特性はGH13 α-グルコシダーゼと，グルコシダーゼIIのグリコン特性はGH31 α-グルコシダーゼと同様であった．またグルコシダーゼIとグルコシダーゼIIのアグリコン認識は同様であり，GH13およびGH31 α-グルコシダーゼとは異なっていた．そこで，プロセシンググルコシダーゼIおよびIIを標的として，酵素阻害剤候補化合物の設計と合成を行った．これら候補化合物の*in vitro*酵素阻害活性と細胞レベルでのウイルス外被糖タンパク質の合成・成熟・転送阻害およびプラーク法による感染性ウイルス数の測定を行った．その結果，*in vitro*においてヘプチトール誘導体，スルフォニル誘導体の一部にIC_{50}約50 μMの阻害活性を，カテキン誘導体の一部にIC_{50} 0.9 μMの強力な阻害活性を見いだした．さらに，細胞レベルではカテキン誘導体の一部にプロセシンググルコシダーゼ阻害を作用点とするとみられる比較的強い抗ウイルス活性を見いだした．今後，ウイルス外被糖タンパク質の糖鎖構造解析等により詳細な作用機序の解明を行う予定である．

*****

〔質 問〕 食総研 徳安

1）安全性の高いカテキン骨格をリード化合物として，カテキン骨格を含む阻害剤の設計と合成を行っていますが，その阻害剤の「安全性が高い」という理由はなにか．

2）ウイルスに対してカテキン誘導体の効果があったが，α-グルコシダーゼに対して作用した結果なのか．

〔答〕

1）誘導体合成前のカテキンの安全性が高いからといって，カテキン骨格を有する誘導体の安全性が高いということはできません．しかし，安全性の高い骨格を創薬リード化合物として用いることは，毒性を回避するという目的において理にかなっていると考えています．また，本誘導体はカテキン骨格をほぼ維持しているので，毒性発現の可能性を低く抑えられるのではないかと考えております．

2）α-グルコシダーゼに対する阻害効果なのかどうか，直接の証拠はありませんが，*in vitro*での強い阻害活性およびウイルスを感染させた培養細胞の形態からα-グルコシダーゼ阻害を作用機序とする抗ウイルス作用であると考えております．今後，ウイルス粒子を回収し，そのウイルス外被糖タンパク質の糖鎖解析を行うことにより，作用点を解明したいと考えております．

〔質 問〕 食総研 北岡

1）グルコシダーゼ阻害剤のリード化合物として，数ある安全性の高い物質の中から，カテキンを選択した理由はなにか．

2）グルコシダーゼ以外の糖質加水分解酵素の阻害剤になっている可能性はあるのでしょうか．

〔答〕

1）安全性の高い物質は他にもたくさんありますが，カテキンには弱いながらも血糖上昇抑制作用が報告されており，腸管グルコシダーゼ阻害が示唆されておりますので，リード化合物として選択いたしました．

2）グルコシダーゼ阻害以外の阻害活性があることは否定できません．現時点では，一部のα-マンノシダーゼに対する阻害活性がないことだけ確認しております．

Available online at www.sciencedirect.com
SCIENCE DIRECT
Bioorganic & Medicinal Chemistry
ELSEVIER
Bioorganic & Medicinal Chemistry 14 (2006) 1437–1443

Structural basis for DNA-cleaving activity of resveratrol in the presence of Cu(II)

Kiyoshi Fukuhara,[a,*] Maki Nagakawa,[b] Ikuo Nakanishi,[c,d] Kei Ohkubo,[d] Kohei Imai,[e] Shiro Urano,[e] Shunichi Fukuzumi,[d] Toshihiko Ozawa,[c] Nobuo Ikota,[c] Masataka Mochizuki,[b] Naoki Miyata[f] and Haruhiro Okuda[a]

[a]*Division of Organic Chemistry, National Institute of Health Sciences, 1-18-1 Setagaya-ku, Tokyo 158-8501, Japan*
[b]*Division of Organic and Bioorganic Chemistry, Kyoritsu University of Pharmacy, 1-5-30 Shibakoen, Minato-ku, Tokyo 105-8512, Japan*
[c]*Redox Regulation Research Group, Research Center for Radiation Safety, National Institute of Radiological Sciences (NIRS), 4-9-1 Anagawa, Inage-ku, Chiba 263-8555, Japan*
[d]*Department of Material and Life Science, Graduate School of Engineering, Osaka University, SORST, Japan Science and Technology Agency (JST), 2-1 Yamada-oka, Suita, Osaka 565-0871, Japan*
[e]*Department of Applied Chemistry, Shibaura Institute of Technology, Minato-ku, Tokyo 108-8548, Japan*
[f]*Graduate School of Pharmaceutical Sciences, Nagoya City University, 3-1 Tanabe-dori, Mizuho-ku, Nagoya, Aichi 467-8603, Japan*

Received 31 August 2005; revised 27 September 2005; accepted 27 September 2005
Available online 24 October 2005

Abstract—Resveratrol (**1**, 3,5,4′-trihydroxy-*trans*-stilbene), a polyphenol found in grapes and other food products, is known as an antioxidant and cancer chemopreventive agent. However, **1** was shown to induce genotoxicity through a high frequency of micronucleus and sister chromatid exchange in vitro and DNA-cleaving activity in the presence of Cu(II). The present study was designed to explore the structure–activity relationship of **1** in DNA strand scission and to characterize the substrate specificity for Cu(II) and DNA binding. When pBR322DNA was incubated with **1** or its analogues differing in the number and positions of hydroxyl groups in the presence of Cu(II), the ability of 4-hydroxystilbene analogues to induce DNA strand scission is much stronger than that of 3-hydroxy analogues. The high binding affinity with both Cu(II) and DNA was also observed by 4-hydroxystilbene analogues. The reduction of Cu(II) which is essential for activation of molecular oxygen proceeded by addition of **1** to the solution of the Cu(II)–DNA complex, while such reduction was not observed with the addition of isoresveratrol, in which the 4-hydroxy group of **1** is changed to the 3-position. The results show that the 4-hydroxystilbene structure of **1** is a major determinant of generation of reactive oxygen species that was responsible for DNA strand scission.

1. Introduction

Natural polyphenols, including catechin, epicatechin, quercetin, and resveratrol, are natural antioxidants that are found in a wide range of plant species. Polyphenols inhibit the oxidation of human low-density lipoprotein (LDL),[1] which is responsible for promoting atherogenesis,[2,3] and the intake of foods and beverages that contain polyphenols may protect against atherosclerosis.[4] The polyphenol resveratrol (3,5,4′-trihydroxy-*trans*-stilbene; **1**) is found in grapes, where it serves as a phytoalexin that protects against fungal infection.[5] Although its biosynthesis is not well defined, **1** is thought to be synthesized in response to infection or injury.[6] Resveratrol **1** (Fig. 1) has some therapeutic effects that are due to its antioxidant potential and originate from the inhibition of the oxidation of human LDL and the reduced propensity of human plasma and LDL to undergo lipid peroxidation.[7,8] In addition to its antioxidant potential, it has also been reported to have a variety of anti-inflammatory, anti-platelet, and anti-carcinogenic effects.[9,10] Therefore, due to its high concentration in grape skin, the beneficial effects of the consumption of red wine at reducing the risk of cardiovascular disease have been attributed to the multiple effects of **1**.[11] Recently, **1** was shown to inhibit cellular events associated with

Keywords: Resveratrol; Polyphenol; Antioxidant; DNA oxidative damage.
* Corresponding author. Tel.: +81-3-3700-1141; fax: +81-3-3707-6950; e-mail: fukuhara@nihs.go.jp

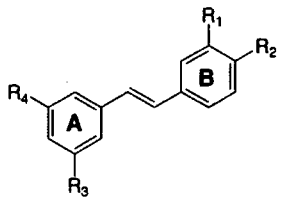

	R_1	R_2	R_3	R_4
1	H	OH	OH	OH
2	OH	H	OH	OH
3	H	H	OH	OH
4	H	OH	OH	H
5	OH	H	OH	H
6	OH	H	H	H
7	H	OH	H	H
8	OH	OH	OH	OH
9	OH	OH	OH	H
$1H_2$	H	OH	OH	OH

Figure 1. Structure of resveratrol (**1**), its analogues **2**–**9**, and dihydroresveratrol (**$1H_2$**).

tumor initiation, promotion, and progression.[12] Furthermore, it has been reported that **1** has the potential to inhibit DNA polymerase and cyclooxygenase,[13] and also has a direct antiproliferative effect on human breast epithelial cells.[14] Based on its antimutagenic activity,[15,16] it has been suggested that **1** should be effective as a cancer chemopreventive agent in humans.

Meanwhile, 5-alkyl-1,3-dihydroxybenzenes (5-alkylresorcinol) have long been recognized to have potential as therapeutic agents, since natural resorcinols have a wide variety of biological activities, including fungicidal and bactericidal activities against numerous pathogens.[17] Hecht and co-workers were the first to demonstrate that 5-alkylresorcinol induced Cu(II)-dependent DNA strand scission under alkaline pH.[18] This DNA cleavage requires the initial oxygenation of the benzene nucleus, a process that occurs readily at an alkaline pH in the presence of Cu(II) and O_2. The resulting trihydroxylated benzene mediates DNA cleavage in a reaction that depends on the presence of Cu(II) and O_2. Recently, based on the similar structures of 5-alkylresorcinol and resveratrol, we suggested that **1** may be able to mediate Cu(II)-dependent DNA strand scission under neutral conditions.[19] Interestingly, DNA strand scission occurred at neutral pH, indicating that **1** can induce DNA cleavage without the oxygenation of benzene nuclei to the catechol moiety, which is a requisite intermediate in resorcinol-induced DNA cleavage. It has also been shown that DNA cleavage is more likely caused by a copper–peroxide complex as the reactive species rather than by a freely diffusible oxygen species that mediates DNA degradation by resorcinol in the presence of Cu(II). However, instead of the catechol structure, the structural feature of **1** that is effective for DNA cleavage is still unknown. To address this question, the present study was designed to explore the structure–activity relationship of synthesized hydroxystilbene derivatives (Fig. 1) in DNA strand 4 scission and also to characterize the substrate specificity for Cu(II) and DNA binding. The results show that the 4-hydroxy group of **1** is a major determinant of DNA cleaving ability and confirm that the stilbene structure is also important for this ability.

2. Result and discussion

2.1. DNA-cleaving activity

The ability of **1** and its analogues to induce DNA-cleaving activity was examined using pBR322, a supercoiled, covalently closed circular DNA (Form I), and analyzed by agarose gel electrophoresis. Consistent with the fact that Cu(II) is required for potent DNA-cleaving activity of **1**, the individual hydroxylated stilbenes induced DNA cleavage only when the reaction was carried out in the presence of Cu(II); in the absence of Cu(II), no DNA cleavage was observed (data not shown). Figure 2 shows the results of the analysis in the presence of Cu(II). Replacement of the internal double bond in the stilbene moiety by a saturated one (**$1H_2$**) resulted in a marked reduction in potency, suggesting that the structure of stilbene is important for mediating DNA relaxation. In a series of hydroxylated stilbene analogues, Cu(II)-dependent DNA-cleaving activity was greatly affected by the number and positions of hydroxyl groups attached to the stilbene structure. For a given structural series (i.e., all 4-OH analogues: **1**, **4**, **7**; 3-OH analogues: **2**, **3**, **5**, **6**; or 3,4-(OH) analogues: **8**, **9**), the DNA-cleaving activity seemed to increase with an increase in the number of hydroxyl groups. Densitometric analysis of agarose gel indicated that the DNA-cleaving ability of **1** resulted not only in the complete conversion of substrate DNA (Form I) into open circular DNA (Form II) but also the further conversion of Form II into linear

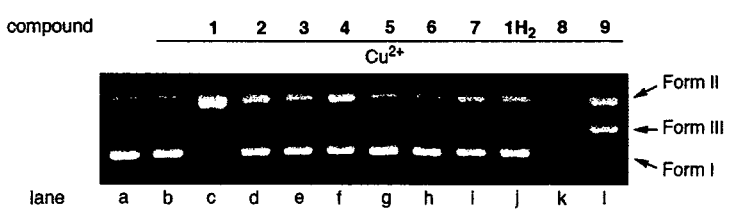

Figure 2. Gel electrophoretic analysis of single- and double-strand breaks generated in pBR322DNA with **1** or its analogues in the presence of Cu(II). Assays were performed in 50 mM sodium cacodylate buffer, pH 7.2, containing 45 μbp pBR322DNA and 10 μM of samples (lane c–l) in the presence of 10 μM Cu(II) (lane b–l), for 1 h at 37 °C. The samples in lane c–l are **1**–**9**, and **$1H_2$**, respectively.

DNA (Form III) in 8% yield. Compounds **8** and **9** were much more efficient at mediating DNA relaxation than **1**; especially, **8** induced the complete degradation of linear DNA (Form III) as indicated by the smearing of the band. The high potency of **8** and **9** can be attributed to their *ortho*-hydroquinone (catechol) structure, which logically improves their ability to cleave DNA by facilitating the generation of oxygen radicals through the formation of *ortho*-hydroquinone–Cu(II)–O_2 complex. Of particular interest is the difference in the potency between **1** and its 3-hydroxy isomer **2**. A change in the placement of the 4-hydroxy group of **1** to the 3-position resulted in a significant decrease in its ability to cleave DNA. Similar differences were noted in comparing the dihydroxy (**4** vs **5**) and monohydroxy (**6** vs **7**) stilbenes, which is consistent with the suggestion that the 4-hydroxy group is essential for effecting DNA cleavage. Since oxygen radical is believed to be the active species responsible for Cu(II)-dependent DNA cleavage, the 4-hydroxy group in combination of O_2 and Cu(II) may serve to facilitate the generation of oxygen radical. However, **3** was found to be quite efficient at mediating DNA relaxation, which suggests that the 3,5-dihydroxybenzene structure, which is distinct from 3-hydroxybenzene, is also essential for potentiating DNA strand scission.

2.2. Cu(II)-binding ability

It has been shown that several xenobiotics that contain a catechol moiety undergo Cu(II)-mediated oxidation to form reactive oxygen species (ROS) that are capable of causing DNA strand breaks. Sotomatsu et al. demonstrated that Cu(II) and Fe(III) had affinity for the hydroquinone moiety of 3,4-dihydroxyphenylalanine (dopa) and, after coordinating with dopa, promoted the peroxidative cleavage of unsaturated phospholipids.[20] Since **1** can coordinate Cu(II), its binding ability has been observed as a change in UV absorption spectra using a Cu(II) titration experiment, whereas no such binding has been observed in the case of Fe(III).[8] Considering the unique specificity of Cu(II), which may induce DNA strand scission of **1**, the ability of **1** to bind to Cu(II) might be advantageous for generating ROS and inducing Cu(II)-dependent DNA scission. Therefore, to elucidate the structural component of **1** that is responsible for its Cu(II)-binding ability, the UV spectra of **1** and its analogues (**2**–**7** and $\mathbf{1H_2}$) in various concentrations of Cu(II) were observed, and their Cu(II)-binding abilities were compared. As shown in Figure 3, the incremental addition of Cu(II) to 20 μM of **1** resulted in a blueshift of the peak from 220 to 210 nm with a concomitant increase in absorbance and a decrease in the absorbance at 308 nm, consistent with the binding of **1** with Cu(II). This spectral change reflects a 1:1 stoichiometry for the complex between **1** and Cu(II), and the binding constant was determined to be $1.75 \times 10^7\ M^{-1}$. Figure 4 shows the effect of the Cu(II) concentration on the absorbance of **1** and its analogues in the range 270–330 nm. A decrease in absorbance, similar to that of **1** at 308 nm, was observed for 3,4- and 4-hydroxy analogues of **4** and **7** at 324 and 304 nm, respectively, indicating that the change is due to its coordination with

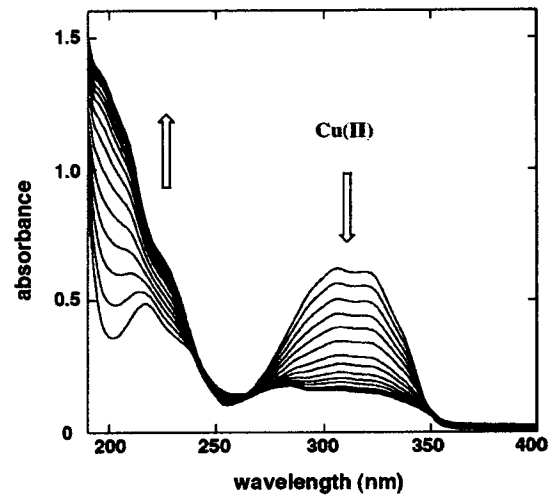

Figure 3. Spectral changes observed upon addition of $CuCl_2$ (0–30 μM) to a sodium cacodylate buffer (pH 7.1)/CH_3CN mixed solution of **1** (20 μM).

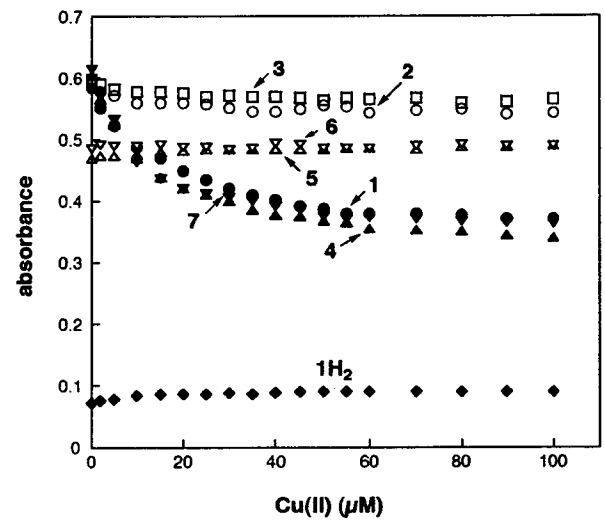

Figure 4. Changes in the absorbance (λ_{max}) of **1** and its analogues (20 μM) upon the addition of $CuCl_2$ (0–100 μM).

Cu(II). In contrast, with an increase in the concentration of Cu(II), there was little or no effect on the absorbance of **2**, **3**, **5**, and **6**, which lacked a 4-hydroxy group on the stilbene moiety, at 306, 300, 298, and 298 nm, respectively, suggesting that ligation of these compounds to Cu(II) did not occur. Further, only a slight effect was observed for dihydroresveratrol $\mathbf{1H_2}$. These results constitute strong evidence that the 4-hydroxy group of **1** is essential for Cu(II) coordination and the ability of the 4-hydroxy group to bind with Cu(II) depends on the structure of stilbene.

2.3. DNA-binding ability

Since **1** is capable of binding to DNA,[19] ROS produced by **1** in combination with Cu(II) might be effective at mediating DNA relaxation. Therefore, to

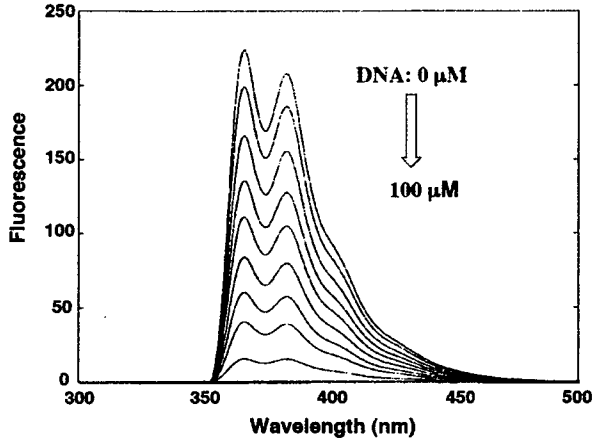

Figure 5. Effect of calf thymus DNA on the fluorescence emission (excitation wavelength 260 nm) of **1**. Trace 1 is the emission spectrum of **1** alone (20 μM); traces 2–9 are emission spectra of **1** in the presence of 2, 5, 10, 15, 20, 30, 50, and 100 μM DNA bp, respectively.

characterize the interaction of **1** with DNA, the ability of **1** and its analogues to bind DNA was estimated by fluorescence titration. The fluorescence emission spectra of **1** in the presence of calf thymus DNA are shown in Figure 5. As indicated, the addition of DNA to **1** causes a decrease in fluorescence emission, and, without any modification of the spectral shape, a decrease in the degree of fluorescence is seen with an increasing concentration of DNA, suggesting that **1** binds to duplex DNA not via groove binding but rather through significant intercalation. In fact, denatured DNA does not appreciably quench the fluorescence of **1** (data not shown). Stern–Volmer plots of the quenching of the fluorescence of **1** and its analogues (**2**–**7** and $\mathbf{1H_2}$) by calf thymus DNA are shown in Figure 6. Native DNA quenches the fluorescence of **1** five times more efficiently than it quenches $\mathbf{1H_2}$,

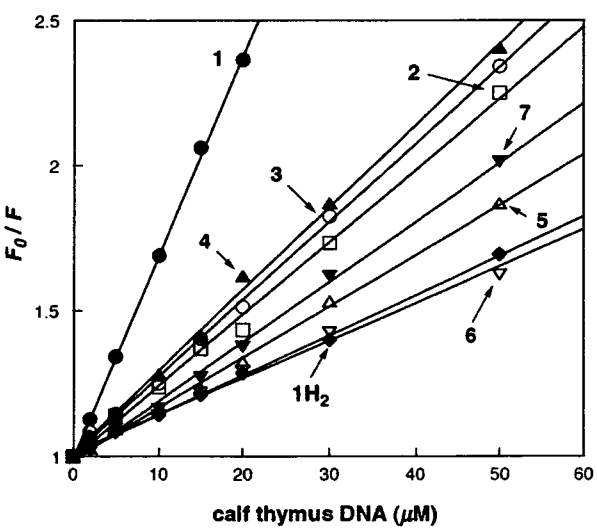

Figure 6. Stern–Volmer plot of quenching of the fluorescence of **1** and its analogues by calf thymus DNA.

indicating that the planarity of the stilbene structure is effective for binding with the duplex DNA structure, probably by taking advantage of its stacking against the base pair. Figure 6 also indicates that phenolic hydroxyl groups attached to the stilbene structure greatly affect the DNA-binding affinity. An increase in the number of hydroxyl groups tends to increase the DNA-binding affinity, which is consistent with the suggestion that the number of phenolic hydroxyl groups is important for its DNA-binding affinity. However, the binding affinity is also determined by the combination of the number and localization of phenolic hydroxyl groups. Thus, the fluorescence of isoresveratrol **2**, in which the 4-hydroxy group of resveratrol **1** is changed to the 3-position, was quenched by DNA with low efficiency ($K_{sv} = 2.40 \times 10^4\ M^{-1}$) compared to **1** ($K_{sv} = 6.80 \times 10^4\ M^{-1}$), and the same results were also observed with dihydroxyl (**4** vs **5**) and monohydroxyl (**7** vs **6**) stilbenes, suggesting that the 4-hydroxy group may be the essential component for binding DNA and plays an important role in specific hydrogen bond interactions with DNA.

2.4. ESR analysis

To confirm the electrostatic interaction of hydroxylated stilbenes with both Cu(II) and DNA, ESR signals of Cu(II) were observed in the presence of **1** or its analogues together with calf thymus DNA. Once the ternary complex of Cu(II)-**1**-DNA, which is due to the efficient binding affinities of **1** with both Cu(II) and DNA, is formed, the complex may result due to its high DNA-cleaving ability. Figure 7 shows that an ESR signal of Cu(II) became multiple upon the addition of DNA, consistent with the fact that Cu(II) complexes DNA. In fact, the decrease in the peak height of Cu(II) in a solution of calf thymus DNA is due to the intercalation of Cu(II) with a large molecule of DNA, which limits the mobility of Cu(II). When **1** was added to the solution of Cu(II)–DNA complex, the peak height of the ESR signal was reduced to one-half of that of the Cu(II)–DNA complex and the resonance was weakened, suggesting that **1** was bound to Cu(II)–DNA complex and thus induced the reduction of Cu(II), which was converted to an ESR-silent species, very likely Cu(I). If the binding of Cu(II) to DNA decreases with the addition of **1**, the signal of Cu(II) should increase to the height of unbound Cu(II). An increase in peak height was also not observed for other resveratrol analogues, suggesting that Cu(II) remains in a complex with DNA even after the addition of **1** and its analogues. Compared to the reduction of Cu(II) to Cu(I) by **1**, an efficient reduction of the peak height of Cu(II)–DNA complex was not observed with the addition of isoresveratrol **2**. It is possible that the insufficient binding affinity of **2** with both DNA and Cu(II) may impair the highly efficient reduction of Cu(II) to Cu(I). Similarly, **7** affected the spectra of Cu(II)–DNA with efficient reducing and broadening, whereas there was no effect on the spectra of Cu(II)–DNA upon the addition of **6**, indicating that the reductive activation of Cu(II) is accelerated by electrostatic interaction of a hydroxyl group at the 4-position.

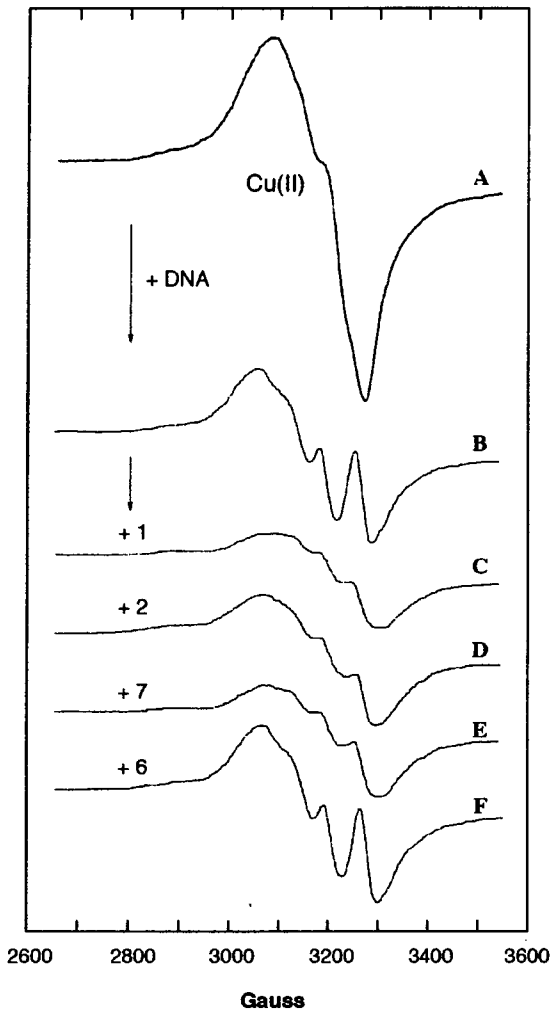

Figure 7. Effect of **1** and its analogues on the ESR spectra of Cu(II) in the presence of calf thymus DNA. Spectra A is 1 mM $CuCl_2$ and spectra B–F show after the addition of 2 mM NP of calf thymus DNA in the absence (B) or presence of 1 mM chemicals (C: **1**; D: **2**; E: **7**; F: **6**). All spectra were recorded after incubation for 30 min at room temperature.

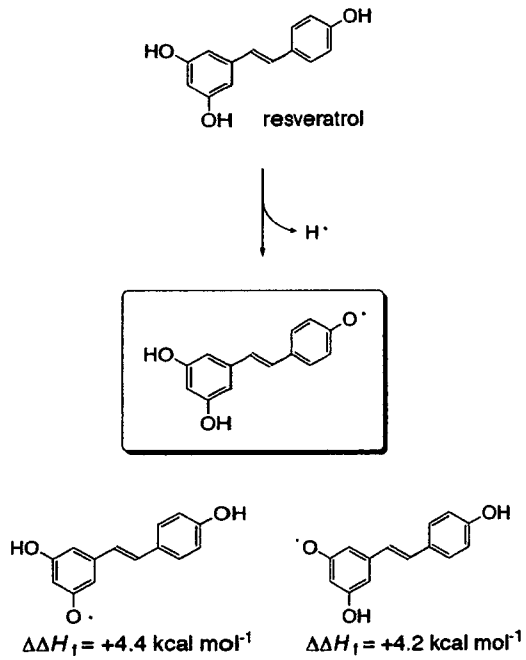

Figure 8. Relative energy values ($\Delta\Delta H_f$) of three types of resveratrol radicals calculated by the DFT calculation, B3LYP/6-31G* basis set.

3. Conclusion

In general, polyphenols, which are responsible for reactive oxygen-associated toxicity, appear to play an important role in the reductive activation of molecular oxygen by its autooxidation, which, in most cases, is coupled with the formation of redox active *ortho*- or *para*-quinones. Catechol is the typical polyphenol that is essential for generating oxygen radical in the presence of Cu(II).[21] It is formed as an activated metabolite of polycyclic aromatic hydrocarbons, which are known to be ubiquitous environmental pollutants. Although **1** is a polyphenol that is known to be an antioxidant and a potential cancer chemopreventive agent, it cleaved DNA strongly without oxidative transformation to the catechol structure in the presence of Cu(II). The DNA cleavage is attributed to the generation of copper-peroxide complex that is formed by electron transfer from **1** to molecular oxygen.[19] The oxidative product of **1** is a dimer[22] and formation of the catechol structure has not been reported. Therefore, the oxidative dimer might be formed by dimerization of resveratrol radical as a result of the reductive activation of molecular oxygen. In the present work, the number and positions of the hydroxyl groups in the stilbene structure were associated with DNA-cleaving activity and the 4-hydroxy group of stilbene played an especially critical role in DNA cleavage. The high binding affinity of a hydroxyl group at the 4-position with both Cu(II) and DNA makes it possible to form a ternary complex and therefore cleave DNA efficiently. When the heats of formation of three types of resveratrol radicals are compared, as shown in Figure 8, the 4-oxyl radical of **1** is the most stable, indicating that the hydroxyl group at the 4-position is much more subjected to oxidation than other hydroxyl groups. In fact, the efficient reduction of Cu(II) to Cu(I) was seen with **1**, which has a hydroxyl group at the 4-position, while there was no effect on Cu(II) reduction in the presence of **2** in which the 4-hydroxy group in **1** is moved to the 3-position. The decrease in the DNA-cleaving ability of $\mathbf{1H_2}$ compared to that of **1** also indicated the importance of the stilbene structure, which might be effective not only for DNA binding for the planarity of the overall structure but also for the stability of the 4-oxyl radical. These results suggest that the ability of **1** to induce oxidative DNA damage in the presence of Cu(II) can be attributed to the structure of 4-hydroxystilbene which is comparable to that of catechol.

Estrogens have been reported to cause cancer through a genotoxic effect. The genotoxicity of estrogens is attributed to the accumulation of potentially carcinogenic metabolites and almost all of these are the catechol form of estrogens. Catechol estrogen metabolites are capable

of causing chromosomal aberrations and gene mutations in cultured cells. The oxidative DNA damage and/or alkylation of DNA that is responsible for the risk of developing cancer are also induced by catechol estrogen metabolites. In fact, the catechol structure, which can cause genotoxicity, is capable of inducing DNA strand scission and the oxidation of DNA bases in the presence of Cu(II). Recently, we reported the genotoxicity of **1**, which induced micronucleus, sister chromatid exchange, and S phase arrest.[23] Among the many types of hydroxylated stilbenes, 4-hydroxystilbene most effectively caused genotoxic effects. Therefore, the finding that the 4-hydroxylstilbene structure is responsible for various biological activities, especially DNA damage leading to genotoxicity, might be important for understanding the toxicity of polyphenols that do not have a catechol structure.

4. Experimental

4.1. Materials

Resveratrol **1** and calf thymus DNA were purchased from Sigma (St. Louis, MO). Supercoiled plasmid pBR322DNA was purchased from Nippon Gene (Tokyo, Japan). Analogues of **1**; 3,5,3′-trihydroxy- (**2**), 3,5-dihydroxy- (**3**), 3,4′-dihydroxy- (**4**), 3,3′-dihydroxy- (**5**), 3-hydroxy- (**6**), 4-hydroxy (**7**), 3,4,3′,5′-tetrahydroxy- (**8**), and 3,4,3′-trihydroxy-*trans*-stilbene (**9**), as shown in Figure 1, were synthesized as previously reported.[24] Saturated form of **1** (**1H$_2$**) was synthesized by hydrogenation of **1** using 10% Pd/C as catalyst. Yield: 98%. ^{1}H NMR(acetone-d_6): δ 2.73 (m, 4H), 6.19 (d, 1H, J = 2.0 Hz), 6.22 (d, 1H, J = 2.0 Hz), 6.74 (d, 2H, J = 8.4 Hz), 7.03 (d, 2H, J = 8.4 Hz). All other chemicals and solvents were of reagent grade or better.

4.2. DNA-cleaving activity

DNA strand breakage was measured in terms of the conversion of supercoiled pBR322 plasmid DNA to the open circular and linear forms. Reactions were carried out in 20 μL (total volume) of 50 mM Na cacodylate buffer (2.5% DMF), pH 7.2, containing 45 μM bp pBR322 DNA, 10 μM $CuCl_2$, and 100 μM of each stilbene derivative. The reaction mixtures were incubated at 37 °C for 1 h and then treated with 5 μL of loading buffer (100 mM TBE buffer, pH 8.3, containing 30% glycerol, 0.1% bromophenol blue) and applied to 1% agarose gel. Horizontal gel electrophoresis was carried out in 50 mM TBE buffer, pH 8.3. The gels were stained with ethidium bromide (1 μg mL^{-1}) for 30 min, destained in water for 30 min, and photographed with UV translumination.

4.3. UV–visible spectra measurements

UV-visible spectra were measured at 37 °C with a Hewlett Packard 8452A Diode Array Spectrophotometer. A solution in a final volume of 1 mL consisted of 20 μM of sample and 0–100 μM $CuCl_2$ in sodium cacodylate buffer (pH 7.1)/acetonitrile mixed solvent (1:1 v/v) was prepared and subjected to spectral analysis. The binding constant between **1** and Cu(II) was obtained according to the method described by Itoh et al.[25]

4.4. Fluorescence measurements

Fluorescence excitation and emission spectra were recorded on a Shimadzu RF-5300PC. A solution in a final volume of 1 mL, which consisted of 20 μM of sample and 0–100 μM calf thymus DNA in 10 mM sodium cacodylate buffer (pH 7.1) and DMF (10% by volume), was used for fluorescence-quenching experiments. The excitation wavelengths used were 255 nm for **1**, **3**, **6**, and **7**, and 260 nm for **2**, **4**, **5**, and **1H$_2$**, and emissions were recorded in the range of 300–500 nm. For all experiments, the sample temperature was maintained at 37 °C. The quenching data were analyzed by the Stern–Volmer equation:[26]

$$F_0/F = 1 + K_{sv}[Q].$$

where [Q] is the molar concentration of the calf thymus DNA, F_0 and F are the fluorescence intensities in the absence and in the presence of the calf thymus DNA [Q], respectively, and K_{sv} is the Stern–Volmer quenching constant.

4.5. ESR analysis

ESR spectra were recorded at room temperature on a JES-FE 2XG spectrometer (JEOL Co. Ltd., Tokyo, Japan). The sample containing 1 mM $CuCl_2$, 2 mM NP of calf thymus DNA, and 1 mM of chemical in 50 mM phosphate buffer (pH 7.2) and acetonitrile (5% by volume) was introduced into a quartz flat cell and incubated at room temperature for 30 min. The ESR spectrum was then recorded. The spectrometer settings were modulation frequency, 100 kHz; modulation amplitude, 10 G; and microwave power, 16 mW.

4.6. Theoretical calculations

Density functional calculations were performed with Gaussian03 (Revision C.02, Gaussian, Inc.) using the unrestricted B3LYP functional for the open shell molecule on an 8-processor QuantumCube™ developed by Parallel Quantum Solutions.

Acknowledgments

This work was supported partly by a grant (MF-16) from the Organization for Pharmaceutical Safety and Research of Japan, a grant from the Ministry of Health, Labour and Welfare, a Grant-in-Aid for Research of Health Sciences focusing on Drug Innovation (KH51058) from the Japan Health Sciences Foundation, and partly by Grants-in-Aid for Scientific Research (B) (No. 17390033) and for Young Scientist (B) (No. 17790044) from the Ministry of Education, Culture, Sports, Science and Technology, Japan.

References and notes

1. Hirano, R.; Sasamoto, W.; Matsumoto, A.; Itakura, H.; Igarashi, O.; Kondo, K. *J. Nutr. Sci. Vitaminol. (Tokyo)* **2001**, *47*, 357.
2. Witztum, J. L.; Steinberg, D. *J. Clin. Invest.* **1991**, *88*, 1785.
3. Steinberg, D. *J. Biol. Chem.* **1997**, *272*, 20963.
4. Hayek, T.; Fuhrman, B.; Vaya, J.; Rosenblat, M.; Belinky, P.; Coleman, R.; Elis, A.; Aviram, M. *Arterioscler. Thromb. Vasc. Biol.* **1997**, *17*, 2744.
5. Jeandet, P.; Bessis, R.; Gautheron, B. *Am. J. Enol. Vitic.* **1991**, *42*, 41.
6. Langcake, P.; Pryce, R. *J. Physiol. Plant Pathol.* **1976**, *9*, 77.
7. Frankel, E. N.; Waterhouse, A. L.; Kinsella, J. E. *Lancet* **1993**, *341*, 1103.
8. Belguendouz, L.; Fremont, L.; Linard, A. *Biochem. Pharmacol.* **1997**, *53*, 1347.
9. Jang, M.; Pezzuto, J. M. *Drugs Exp. Clin. Res.* **1999**, *25*, 65.
10. Olas, B.; Wachowicz, B.; Stochmal, A.; Oleszek, W. *Platelets* **2002**, *13*, 167.
11. Wu, J. M.; Wang, Z. R.; Hsieh, T. C.; Bruder, K. L.; Zou, J. G.; Huang, Y. Z. *Int. J. Mol. Med.* **2001**, *8*, 3.
12. Jang, M.; Cai, L.; Udeani, G. O.; Slowing, K. V.; Thomas, C. F.; Beecher, C. W.; Fong, H. H.; Farnsworth, N. R.; Kinghorn, A. D.; Mehta, R. G.; Moon, R. C.; Pezzuto, J. M. *Science* **1997**, *275*, 218.
13. Jang, M.; Pezzuto, J. M. *Drug Exp. Clin. Res.* **1999**, *25*, 65.
14. Mgbonyebi, O. P.; Russo, J.; Russo, I. H. *Int. J. Oncol.* **1998**, *12*, 865.
15. Uenobe, F.; Nakamura, S.; Miyazawa, M. *Mutat. Res.* **1997**, *373*, 197.
16. Kim, H. J.; Chang, E. J.; Bae, S. J.; Shim, S. M.; Park, H. D.; Rhee, C. H.; Park, J. H.; Choi, S. W. *Arch. Pharm. Res.* **2002**, *25*, 293.
17. Lindenberg, B. A.; Massin, M. J. *J. Physiol. (Paris)* **1957**, *49*, 285.
18. Scannell, R. T.; Barr, J. R.; Murty, V. S.; Reddy, K. S.; Hecht, S. M. *J. Am. Chem. Soc.* **1988**, *110*, 3650.
19. Fukuhara, K.; Miyata, N. *Bioorg. Med. Chem. Lett.* **1998**, *8*, 3187.
20. Sotomatsu, A.; Nakano, M.; Hirai, S. *Arch. Biochem. Biophys.* **1990**, *283*, 334.
21. Seike, K.; Murata, M.; Oikawa, S.; Hiraku, Y.; Hirakawa, K.; Kawanishi, S. *Chem. Res. Toxicol.* **2003**, *16*, 1470.
22. Wang, M.; Jin, Y.; Ho, C.-T. *J. Agric. Food Chem.* **1999**, *47*, 3974.
23. Matsuoka, A.; Takeshita, K.; Furuta, A.; Ozaki, M.; Fukuhara, K.; Miyata, N. *Mutat. Res.* **2002**, *521*, 29.
24. Thakkar, K.; Geahlen, R. L.; Cushman, M. *J. Med. Chem.* **1993**, *36*, 2950.
25. Itoh, S.; Taniguchi, M.; Takada, N.; Nagatomo, S.; Kitagawa, T.; Fukuzumi, S. *J. Am. Chem. Soc.* **2000**, *122*, 12087.
26. Barcelo, F.; Barcelo, I.; Gavilanes, F.; Ferragut, J. A.; Yanovich, S.; Gonzalez-Ros, J. M. *Biochim. Biophys. Acta* **1986**, *884*, 172.

Drug Metab. Pharmacokinet. 21 (4): 315-323 (2006).

Regular Article

Chenodeoxycholic Acid-mediated Activation of the Farnesoid X Receptor Negatively Regulates Hydroxysteroid Sulfotransferase

Masaaki MIYATA[1,*] Yoshiki MATSUDA[1], Hiroyuki TSUCHIYA[1], Hirotaka KITADA[1], Takanori AKASE[1], Miki SHIMADA[1], Kiyoshi NAGATA[1], Frank J. GONZALEZ[2] and Yasushi YAMAZOE[1,3]

[1]*Division of Drug Metabolism and Molecular Toxicology, Graduate School of Pharmaceutical Sciences, Tohoku University, Sendai, Japan*

[2]*Laboratory of Metabolism, National Cancer Institute, National Institutes of Health, Bethesda, MD, USA*

[3]*CRESCENDO, The Tohoku University 21st Century "Center of Excellence" Program, Sendai, Japan*

Full text of this paper is available at http://www.jstage.jst.go.jp/browse/dmpk

Summary: Hydroxysteroid sulfotransferase catalyzing bile acid sulfation plays an essential role in protection against lithocholic acid (LCA)-induced liver toxicity. Hepatic levels of Sult2a is up to 8-fold higher in farnesoid X receptor-null mice than in the wild-type mice. Thus, the influence of FXR ligand (chenodeoxycholic acid (CDCA) and LCA) feeding on hepatic Sult2a expression was examined in FXR-null and wild-type mice. Hepatic Sult2a protein content was elevated in FXR-null and wild-type mice fed a LCA (1% and 0.5%) diet. Treatment with 0.5% CDCA diet decreased hepatic Sult2a to 20% of the control in wild-type mice, but increased the content in FXR-null mice. Liver Sult2a1 (St2a4) mRNA levels were reduced to 26% in wild-type mice after feeding of a CDCA diet, while no decrease was observed on Sult2a1 mRNA levels in FXR-null mice after CDCA feeding. A significant inverse relationship ($r^2 = 0.523$) was found between hepatic Sult2a protein content and small heterodimer partner (SHP) mRNA level. PCN-mediated increase in Sult2a protein levels were attenuated by CDCA feeding in wild-type mice, but not in FXR-null mice. Human SULT2A1 protein and mRNA levels were decreased in HepG2 cells treated with the FXR agonists, CDCA or GW4064 in dose-dependent manners, although SHP mRNA levels were increased. These results suggest that SULT2A is negatively regulated through CDCA-mediated FXR activation in mice and humans.

Key words: hydroxysteroid sulfotransferase; FXR; bile acid; sulfation; negative regulation; Sult2a

Introduction

Sulfotransferases (SULT) are phase II metabolizing enzymes that catalyzes sulfation of various endogenous and exogenous chemicals.[1,2] Hydroxysteroid sulfotransferase (SULT2A) is a cytosolic enzyme expressed abundantly in enterohepatic tissues such as liver and intestine, and also in steroidogenic tissue such as the adrenal cortex.[3] SULT2A catalyzes the sulfation of drugs, environmental chemicals and endogenous steroids such as dehydroepiandrosterone (DHEA), estrogen and bile acids.[4,5] SULT2A-mediated sulfation increases the hydrophilicites of bile acids and facilitates their clearance from the body. Because bile acid sulfation is a main metabolic pathway for bile acid excretion, SULT2A is a critical enzyme for bile acid homeostasis. About 95% of bile acids excreted in bile are reabsorbed in the intestine and thus changes in the level of hepatic SULT2A can disrupt bile acid homeostasis in enterohepatic tissues. SULT2A is also considered to play a major role in the protection against toxic bile acid-induced liver injury in enterohepatic tissues. SULT2A preferably catalyzes the sulfation of hydrophobic and toxic bile acids such as LCA. A protective role of Sult2a against LCA-induced hepatotoxicity was demonstrated by using farnesoid X receptor (FXR)-null female mice constitutively expressing higher levels of Sult2a protein.[6] The increase in the production of hepatic Sult2a-

Received; February 13, 2006, Accepted; April 7, 2006

**To whom correspondence should be addressed*: Masaaki MIYATA, Ph.D., *Division of Drug Metabolism and Molecular Toxicology, Graduate School of Pharmaceutical Sciences, Tohoku University, 6-3, Aoba, Aramaki, Aoba-ku, Sendai, 980-8578, Japan. Tel. +81-22-795-6829, Fax. +81-22-795-6826, E-mail: miyata@mail.pharm.tohoku.ac.jp*

mediated 3α-sulfated TLCA and the efficient fecal excretion contributes to the protection against LCA-induced toxicity (submitted for publication).

Two Sult2a mRNAs (Sult2a1 (St2a4) and Sult2a2 (St2a9)) that share high homology, were isolated from mice[7,8] and one mRNA (SULT2A1) has been isolated from humans.[5,9,10]. Mouse Sult2a enzymes are expressed to higher extents in the female. Because of the efficient bile acid sulfating activity in female mice as well as humans, female mice represent a feasible model for bile acid sulfation in humans.

FXR, a member of the nuclear receptor superfamily, is expressed abundantly in liver, intestine and adrenal.[11] The involvement of FXR in bile acid and lipid homeostasis was demonstrated by using FXR-null mice.[12] FXR is activated by several bile acids such as CDCA.[13-15] FXR regulates a variety of genes involved in the metabolism and transport of the lipids such as bile acid and cholesterol. FXR stimulates the expression of Bsep, small heterodimer partner (SHP) and Mrp2, whereas FXR directly represses the expression of apolipoprotein A-I and apolipoprotein C-III, and indirectly suppresses the expression of CYP7A1 and Ntcp through the induction of SHP.[16-18]

CDCA activation of FXR has been shown to stimulate rat SULT2A1 transcription via the FXR response element (IR0) in HepG2 cells.[19]. Furthermore, it was demonstrated that pregnane X receptor (PXR), constitutive androstane receptor (CAR) and vitamin D receptor (VDR) also bind the rat and mouse IR0 elements and enhance the reporter gene activity.[20-23] The Sult2a expression level, however, was increased in FXR-null and PXR-null female mice as compared with that of wild-type mice.[6]

In the present study, SULT2A expression levels were determined using FXR-null mice and HepG2 cells to clarify the involvement of FXR signaling in the suppression of SULT2A gene expression. These results suggest that SULT2A is negatively regulated by activation of FXR with CDCA.

Materials and Methods

Materials: CDCA, LCA, tauroLCA (TLCA), glycoLCA (GLCA), cholic acid (CA), deoxycholic acid (DCA), ursodeoxycholic acid (UDCA), pregnenolone 16α-carbonitrile (PCN) and dehydroepiandrosterone (DHEA) were purchased from Sigma-Aldrich Co. (St. Louis, MO). GW4064 was kindly provided by Dr. Timothy M. Willson (GlaxoSmithKline, Research Triangle Park, NC).

Animal treatment and sample collection: FXR-null female mice[12] were housed under standard 12-h light/12-h dark cycle. Prior to the administration of special diets, the mice were fed standard rodent chow (CE-2, Clea Japan) and water ad libitum for acclimation. Age-matched groups of 8- to 12-week-old animals were used for all experiments. The mice were fed the control diet (CE-2) mixed with 0.5% and 1.0% (w/w) LCA for 9 days or 0.5% CDCA for 5 days. The mice were fed the control diet or the diet mixed with 0.5% (w/w) CDCA for 5 days and injected with PCN (100 mg/kg, ip) for the last 3 days.

Hepatic bile acid concentration: Hepatic 3α-hydroxy bile acid concentrations were estimated by an enzyme-colorimetric method using the Total bile acid-test kit from Wako (Wako Pure Chemicals, Osaka, Japan). Hepatic LCA and CDCA contents were measured by HPLC as previously described.[24]

Cell culture: HepG2 cells were plated in 10 cm culture dishes (Falcon Scientific Co., Oxnard, CA) at 3×10^6 cells and cultured in Dulbecco's modified Eagle's medium (DMEM) containing 10% fetal calf serum. The cells were cultured for 24-h and then treated with CDCA, GW4064 or vehicle (DMSO) for 48-h. The cells were cultured in serum-free DMEM during chemical treatment.

Immunoblot analysis: Cytosolic proteins (30 μg/lane) were loaded onto a 9% polyacrylamide gel, isolated and transferred to nitrocellulose filters. The filter was immunostained with a polyclonal antibody prepared against the purified recombinant rat SULT2A1 protein (1:1000 dilution) that reacts with mouse Sult2a[25] and a polyclonal antibody against the purified recombinant human SULT2A1 protein[26] (1:1000 dilution) for human SULT2A1. The stained filters were scanned with an Epson GT-8700 scanner, and the band intensities measured by use of the NIH image (version 1.59) software (Bethesda, MD).

Expression and purification of Sult2a proteins: Mouse Sult2a cDNAs were obtained from wild-type mouse liver by reverse transcription-polymerase chain reaction (RT-PCR). Sult2a cDNA fragments, containing a sequence of the recognition site of enterokinese next to the N-terminal methionine of the native form, were obtained by RT-PCR and ligated into the prokaryotic expression vector, pQE30 (QIAGEN). The plasmid DNA was transformed into *Escherichia coli*, M15 (pREP4). Recombinant Sult2a proteins were expressed and purified from bacterial cytosols by nickel-nitrilotriacetic acid affinity chromatography. The fused portion of recombinant Sult2a proteins was removed to yield native proteins for standard of immunoblot analyses by enterokinase.

Analysis of mRNA levels: Total RNAs were prepared from livers and HepG2 cells using the RNAgents Total RNA Isolation System (Promega, Madison, WI), and RNA concentrations were determined by measuring the absorbance at 260 nm using a spectrophotometer (Beckman DU 640). Messenger RNA levels of differentially expressed genes were analyzed

using RT-PCR as previously described.[24] Single strand cDNAs were constructed using an oligo(dT) primer with the Ready-to-Go You-Prime First-strand Beads kit (Amersham Pharmacia Biotech AB, Uppsala, Sweden). These cDNAs provided templates for PCRs using specific primers at a denaturation temperature of 94°C for 30 sec, an annealing temperature of 57°C–61°C (61°C for Sult2a1) for 30 sec, and an elongation temperature of 72°C for 30 sec in the presence of dNTPs and Taq polymerase. The PCR cycle numbers were titrated for each primer pair to assure amplification in linear range. The reaction was completed at 7 min incubation at 72°C and PCR products were analyzed in a 2% agarose gel (w/v) containing ethidium bromide for visualization. Their intensities were measured by use of the NIH image (version 1.59) software (Bethesda, MD). The specific forward and reversal primers for the genes examined by PCR were

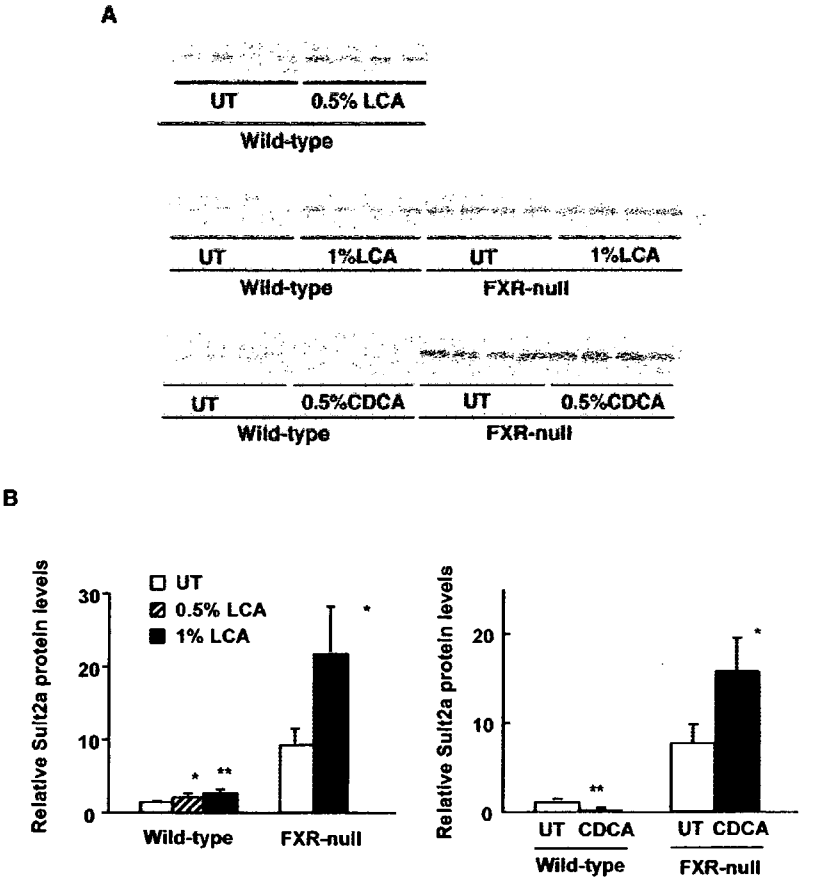

Fig. 1. Influence of bile acid feeding on hepatic Sult2a protein expression levels.

A. Immunoblot analyses of hepatic Sult2a proteins. Hepatic cytosol was prepared from FXR-null and wild-type mice fed a LCA diet for 9 days or fed a CDCA diet for 5 days. Hepatic cytosols (30 μg) were analyzed by immunoblotting with antibody to rat SULT2A1. Intensified staining was shown on the top. B. Quantification of hepatic Sult2a protein levels of mice fed a LCA diet, or a CDCA diet. Data are shown as the mean ± S.D. (n = 4). *, significant difference from control group ($p < 0.05$). **, ($p < 0.01$). UT, untreated.

Table 1. Primers for RT-PCR

Gene	Forward Primer	Reverse Primer
mGAPDH	5′-TGCATCCTGCACCACCAACTG-3′	5′-GTCCACCACCCTGTTGCTGTAG-3′
mSult2a1	5′-CGATCTATCTCGTGAGAAATCCC-3′	5′-TCTCTTCATAGTACAGTACCAAA-3′
mSHP	5′-CTAGCCAAGACACTAGCCTTCC-3′	5′-TTCAGTGATGTCAACGTCTCC-3′
hGAPDH	5′-TTCAACGGCACAGTCAAGG-3′	5′-CACACCCATCAAACATG-3′
hSHP	5′-GCTGTCTGGAGTCCTTCTGG-3′	5′-GAGCCTCCTGCTGCAGGTGC-3′
hSULT2A1	5′-TGGACAAAGCACAACTTCTG-3′	5′-TTATTCCCCATGGGAACAGCTC-3′

m; mouse, h; human.

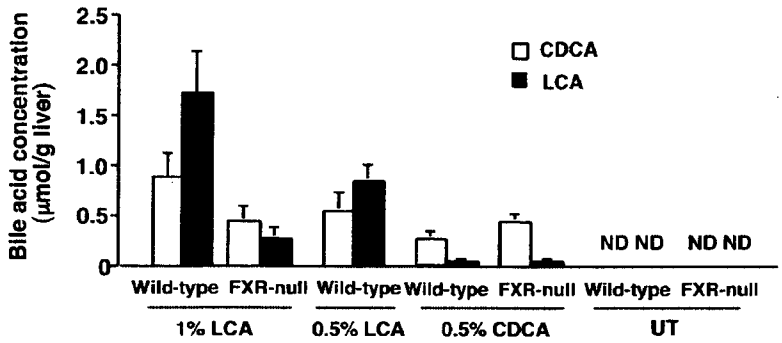

Fig. 2. Hepatic LCA and CDCA concentrations in bile acid-fed mice.
Liver homogenates were prepared from FXR-null and wild-type mice fed a LCA diet for 9 days or fed a CDCA diet for 5 days. Hepatic LCA and CDCA concentrations were determined by HPLC. Combined amounts of tauro and free forms are shown. Data are shown as the mean ± S.D. (n = 4). ND, not detected. UT, untreated.

shown in **Table 1.**

Statistical analysis: All values are expressed as the means ± SD. All data were analyzed by unpaired Student's *t* test or Dunnett's multiple comparisons test for significant differences between the mean values of each group.

Results

Influence of bile acid feeding on hepatic content of Sult2a protein: Hepatic Sult2a expression levels were increased in FXR-null and PXR-null female mice as compared to their wild-type counterparts.[6] Hepatic contents of Sult2a protein in bile acid-treated mice were determined by immunoblotting using rat SULT2A1 antibody to assess the influence of the bile acid-related nuclear receptors in hepatic Sult2a expression. Consistent with our previous data, Sult2a protein contents were markedly higher in livers of FXR-null female mice than in wild-type mice (**Fig. 1A, B**). Hepatic Sult2a protein contents were increased 2.4-fold in wild-type mice fed a 1% LCA diet. The Sult2a contents were also increased 1.8-fold in wild-type mice fed a 0.5% LCA diet. Significant increases (2.4-fold) in Sult2a protein contents were also observed in FXR-null nice fed a 1% LCA diet. Hepatic Sult2a protein contents were markedly decreased to 20% of control in wild-type mice fed a 0.5% CDCA diet (**Fig. 1B**). In contrast to wild-type mice, Sult2a was significantly increased 2.1-fold in FXR-null mice after feeding CDCA.

Hepatic LCA and CDCA concentrations: To understand the mechanism of the change in hepatic Sult2a expression in bile acid-fed mice, hepatic LCA and CDCA concentrations were measured in mice fed a LCA or CDCA diet. FXR-null female mice constitutively expressing high levels of Sult2a protein did not accumulate LCA in livers.[6] As expected, hepatic LCA concentrations were 6.9-fold higher in wild-type mice than in FXR-null mice after feeding a 1% LCA diet for 9 days (**Fig. 2**). In addition, CDCA was detected as the major bile acid in livers of FXR-null and wild-type mice fed LCA (0.5% and 1%) diets. In the FXR-null mice fed a 1% LCA diet, hepatic CDCA concentrations were higher than LCA. Furthermore, hepatic LCA concentrations were 3.4-fold higher in wild-type mice fed a 0.5 % LCA diet than in FXR-null mice fed a 1% LCA diet. In CDCA fed mice, CDCA was detected as the main bile acid component in liver together with trace amounts of LCA. Hepatic CDCA concentrations were 1.8-fold higher in FXR-null mice fed a 0.5% CDCA diet than those in wild-type mice. Hepatic levels of LCA and CDCA in FXR-null and wild-type mice fed a control diet were below the detection limits under our conditions.

Expression and characterization of mouse Sult2a1 and Sult2a2: Two distinct mRNAs of mouse Sult2a were isolated from C57BL/6 wild-type mice by RT-PCR. One matched with Sult2a1 (Accession Number:L02335), and the other showed two nucleotide differences from the reported Sult2a2 cDNA (Accession Number:L27121) isolated from BALB/c mice. This cDNA was judged to correspond to Sult2a2 in the C57BL/6 strain. Although a clear correlation between individual cytosolic LCA sulfation activity and Sult2a protein content was demonstrated,[6] the correspondence between Sult2a mRNA and protein remained unclear. Thus, recombinant Sult2a (Sult2a1 and Sult2a2) proteins were expressed in *Escherichia coli*. The recombinant Sult2a1 protein showed the same electrophoretic mobility on SDS-PAGE as the major cytosolic Sult2a protein detected by antibody generated against rat SULT2A1, whereas the recombinant Sult2a2 protein exhibited a mobility different from the cytosolic Sult2a protein (data not shown). These results indicate that Sult2a protein quantified by Western blotting corresponds to Sult2a1.

Hepatic Sult2a1 mRNA levels in CDCA fed mice:

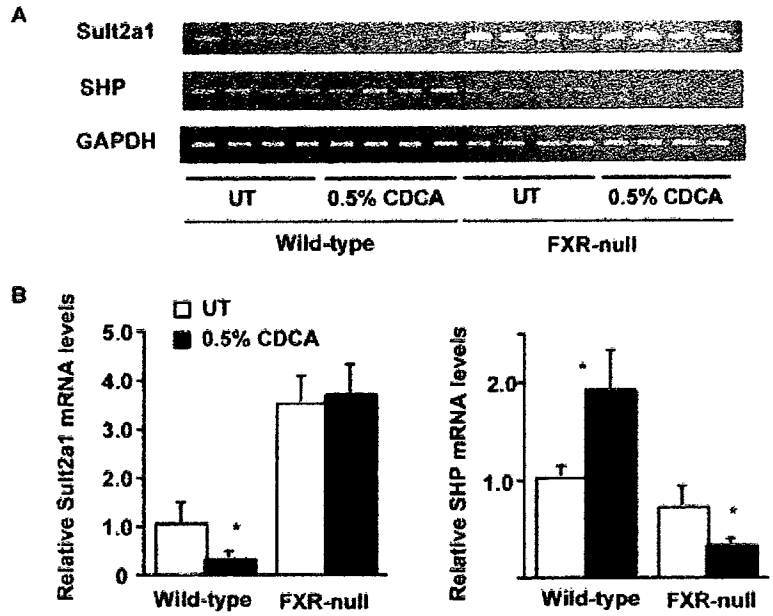

Fig. 3. Influence of CDCA feeding on expression levels of Sult2a1 and SHP mRNAs.

A. Changes in mRNA levels of hepatic mouse Sult2a1 and mouse SHP were analyzed by RT-PCR. Hepatic mRNAs were prepared from FXR-null and wild-type mice fed a 0.5% CDCA diet for 5 days. Specific primers described in **Table 1** were used. B. Quantification of Sult2a1 and SHP mRNA levels. Data are shown as the mean ± S.D. (n = 4). *, significant difference from control group ($p < 0.05$). UT, untreated.

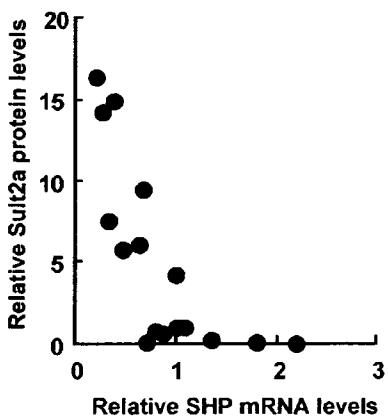

Fig. 4. Relationship between hepatic Sult2a protein and SHP mRNA levels.

Data on FXR-null and wild-type mice fed a 0.5% CDCA diet or a control diet are indicated.

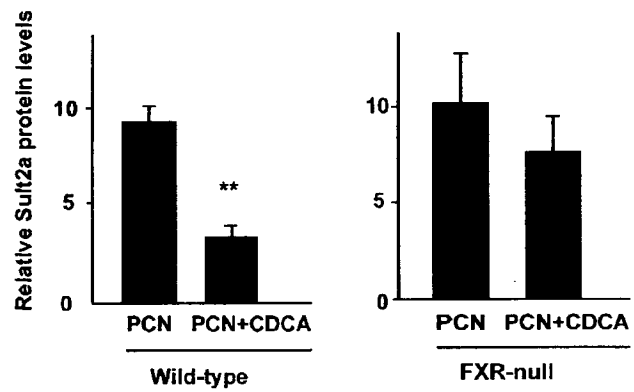

Fig. 5. Influence of CDCA feeding on Sult2a expression in PCN-treated mice.

Wild-type mice and FXR-null mice were fed a control diet or the diet containing 0.5% CDCA for 5 days and injected with PCN (100 mg/kg, ip) the last 3 days. Hepatic cytosols were analyzed by immunoblotting with antibody to rat SULT2A1. The expression level of Sult2a protein was normalized to that of control wild-type mice. Data are shown as the mean ± S.D. (n = 4). **, significant difference from corresponding PCN-treated groups ($p < 0.01$).

Hepatic contents of Sult2a protein were higher in female FXR-null mice than in the corresponding wild-type mice. These results suggest the possibility that FXR mediated suppression of Sult2a expression. Clear decreases in hepatic Sult2a content in CDCA-fed mice further support this finding. Liver Sult2a1 mRNA level was detected by RT-PCR. Under the conditions employed, Sult2a2 mRNA was undetectable. Hepatic levels of Sult2a1 mRNA were reduced to 26% of the wild-type control in mice fed a CDCA diet, which was consistent with the change in Sult2a protein levels. However, no significant decrease in Sult2a1 mRNA levels were observed in the FXR-null mice fed a CDCA diet (**Fig. 3A, B**). As expected, the prototypical FXR target gene, SHP mRNA levels were increased 1.9-fold in wild-type mice fed a CDCA diet. The same treatment decreased SHP mRNA levels in FXR-null mice, suggest-

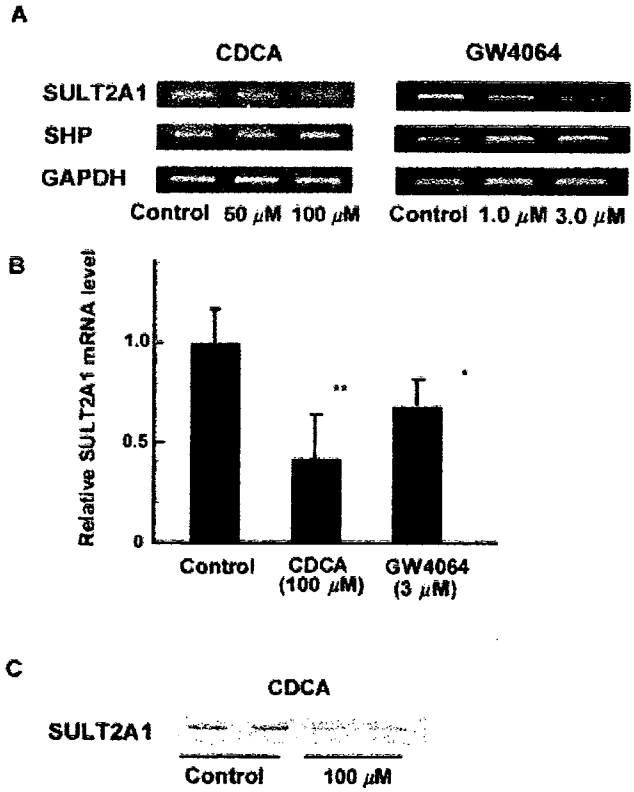

Fig. 6. Influence of FXR agonist on expression levels of human SULT2A1 mRNA and protein in HepG2 cells.

Total mRNAs and cytosols were prepared from HepG2 cells treated with CDCA, GW4064 or vehicle (DMSO) for 48 hrs. A. Human SULT2A1 and SHP mRNA levels. Human SULT2A1 and SHP mRNA levels were analysed by RT-PCR using specific primers described in **Table 1**. B. Relative SULT2A mRNA levels. The levels were analysed by conventional PCR method. Data are shown as the mean ± S.D. (n=4). *, significant difference from control group ($p<0.05$). **, ($p<0.01$). C. Human SULT2A1 protein contents. Human SULT2A1 protein was detected by immunoblots with antibody to human recombinant SULT2A1.

ing a CDCA-mediated suppression of SHP expression. A significant inverse relationship ($r^2=0.523$) was found between Sult2a protein levels and SHP mRNA levels (**Fig. 4**). Furthermore, r^2 value is increased to 0.672 if two points that show more than 1.5 of SHP mRNA level are omitted.

Influence of CDCA feeding on Sult2a expression in PCN-treated wild-type mice: Rodent SULT2A in liver is increased after treatment with PXR ligands such as dexamethasone and PCN.[27] Thus, the influence of CDCA feeding on Sult2a induction by PCN was examined. Sult2a protein contents were increased 9.0-fold in PCN-treated wild-type mice, compared to those in control mice. (**Fig. 5**). The contents were reduced in PCN-treated wild-type mice fed a 0.5% CDCA diet to 35% level of PCN-treated wild-type mice fed a control diet. On the other hand, no significant differences in Sult2a contents were observed between both the groups in FXR-null mice.

Human SULT2A1 expression in HepG2 cells: The influence of FXR agonists on human SULT2A1 levels in HepG2 cells was assessed to determine whether human SULT2A1 was also negatively regulated by FXR signaling. Human SULT2A1 mRNA levels were significantly decreased in HepG2 cells after addition of CDCA in a dose-dependent manner (**Fig. 6A, B**). In contrast, SHP mRNA levels were increased in these cells. These results are consistent with the *in vivo* data in the mice fed a 0.5% CDCA diet. Human SULT2A1 mRNA levels were also decreased in HepG2 cells treated with GW4064, a selective nonsteroidal FXR agonist. Human SULT2A1 protein levels were also decreased in HepG2 cells after addition of 100 μM of CDCA (**Fig. 6C**).

Discussion

The present study demonstrates that SULT2A is negatively regulated by CDCA signaling *in vivo*. The negative influence of CDCA feeding on Sult2a expression is likely to be FXR-dependent as suggested by the inverse relationship ($r^2=0.523$) between levels of SHP mRNA and Sult2a protein. Human SULT2A1 mRNA levels were also reduced in HepG2 cells after treatment with CDCA or GW4064, similar to the results obtained with mouse Sult2a1 expression *in vivo*. Consistent with these results, human SULT2A1 mRNA levels are decreased in cultured human primary hepatocytes treated with CDCA.[28] Although some differences in transcriptional regulation has been demonstrated in rodent and human SULT2A genes, human SULT2A1 expression is also likely to be suppressed by CDCA activation of FXR. However, it cannot be excluded that a CDCA-mediated FXR-independent mechanism such as the c-Jun *N*-terminal kinase (JNK) signaling[29,30] plays a role in suppression of SULT2A expression.

It should also be noted that Sult2a protein contents were increased in mice fed a LCA diet, thus supporting the view that Sult2a is involved in protection against LCA-induced toxicity through sulfation of LCA. LCA serves as an agonist for PXR and VDR[31-33] and it was shown that transcription of rodent SULT2A is positively regulated by several nuclear receptors such as PXR, CAR, VDR and PPARα.[20-23,28,34,35] Thus, hepatic Sult2a protein is likely at least in part induced by PXR and CAR signaling through LCA.

Although 3- to 4-fold higher hepatic LCA concentrations were observed in wild-type mice fed a 0.5% LCA diet, as compared to LCA in FXR-null mice fed a 1% LCA diet, the extents of increase in Sult2a protein was lower in the former mice than that in the latter. These results also support the idea that CDCA-mediated FXR activation negatively regulates hepatic Sult2a expression because CDCA as well as LCA were detected as the